Nanoscale Advances

ROYAL SOCIETY OF CHEMISTRY

REVIEW

View Article Online
View Journal | View Issue

Cite this: *Nanoscale Adv.*, 2023, **5**, 2394

Recent advances in supramolecular self-assembly derived materials for high-performance supercapacitors

Honghong Cheng, * Ruliang Liu, Ruyi Zhang, Lan Huang and Qiaoyi Yuan

The key preponderance of supramolecular self-assembly strategy is its ability to precisely assemble various functional units at the molecular level through non-covalent bonds to form multifunctional materials. Supramolecular materials have the merits of diverse functional groups, flexible structure, and unique self-healing properties, which make them of great value in the field of energy storage. This paper reviews the latest research progress of the supramolecular self-assembly strategy for the advanced electrode materials and electrolytes for supercapacitors, including supramolecular self-assembly for the preparation of high-performance carbon materials, metal-based materials and conductive polymer materials, and its beneficial effects on the performance of supercapacitors. The preparation of high performance supramolecular polymer electrolytes and their application in flexible wearable devices and high energy density supercapacitors are also discussed in detail. In addition, at the end of this paper, the challenges of the supramolecular self-assembly strategy are summarized and the development of supramolecular-derived materials for supercapacitors is prospected.

Received 30th January 2023
Accepted 10th April 2023

DOI: 10.1039/d3na00067b

rsc.li/nanoscale-advances

1. Introduction

Supercapacitors have gained much attention in the last two decades as a new type of energy storage device. The energy density of supercapacitors is 3–4 times higher than that of traditional physical capacitors. Compared with secondary batteries, supercapacitors possess higher power density (300–5000 W kg^{-1}) and long cycle life (>1 million cycles). In addition, supercapacitors also have the advantages of safety and environmental friendliness.[1–4] These characteristics make supercapacitors widely used in electric vehicles, aerospace, smart grids, civil 3C digital and national defense technology, *etc.*[5–7] Generally, according to the energy storage mechanism supercapacitors can be divided into two categories: electrochemical double-layer capacitors (EDLCs) with porous activated carbon as the electrode material, which mainly store energy through the fast and reversible double-layer capacitor at the electrode/electrolyte interface[8–10] and Faraday pseudocapacitors with metal-based materials or conducting polymers as electrodes, which mainly store energy through a rapidly reversible Faraday process at the electrode/electrolyte interface.[9,11] The electrode material is the core factor that determines the performance of supercapacitors. The most widely studied

School of Chemistry and Materials Science, Guangdong University of Education, Guangzhou 510800, P.R. China. E-mail: chenghonghong@gdei.edu.cn

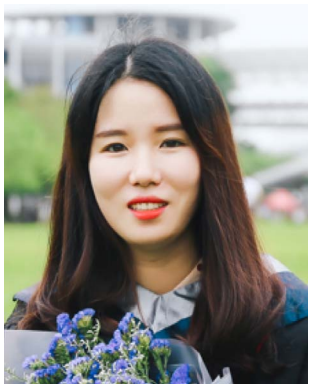

Honghong Cheng received her PhD (2019) from South China Normal University. She is currently working as a lecturer in Guangdong University of Education. Her research interest is focused on the preparation and properties of advanced supercapacitor electrodes.

Ruliang Liu received his PhD (2014) from University of Chinese Academy of Sciences and then worked for two years as a post-doctor in Graduate School at Shenzhen, Tsinghua University. He is currently working as a lecturer in Guangdong University of Education. His research interest is focused on the synthesis of polymer materials for electrochemical energy storage devices.

electrode materials can be classified into three categories: carbon based materials,[12–14] metal oxide materials,[15,16] and conductive polymer materials,[17–19] each of which possesses its inherent advantages and shortcomings. Carbon-based materials, such as porous activated carbon and graphene, possess high conductivity and large specific surface area, and have been commercialized on a large scale.[20,21] However, the limitations of their own structures (for example, the mismatch between the diameter of electrolyte ions and the pore size of porous activated carbon, and the unavoidable aggregation of the individual nanosheets of graphene) usually lead to the low energy density of carbon materials. The metal oxide materials have high theoretical capacity but insufficient conductive properties and cycling stability.[22,23] Conductive polymers also possess high specific capacitance but insufficient conductive properties and cycling stability.[24–26] The above shortcomings seriously limit the application of metal oxides and conductive polymers in the field of supercapacitors. Obtaining high energy density and developing advanced electrode materials with high conductivity and capacitance are key to realizing high performance supercapacitors. Generally, the power and energy density of electrode materials can be significantly improved by combining the EDLC effect and pseudo capacitance effect. Doping heteroatoms into carbon materials can introduce extra pseudocapacitive active sites, which can significantly improve the specific capacitance of carbon-based materials.[27–31] Conductive polymers or metal oxides can also be combined with high electrical conductivity carbon materials to achieve the purpose of complementary advantages.[32–34] The common methods such as the hydrothermal method, electrodeposition, co-precipitation and sol–gel method used in the preparation of heteroatom doped carbon and composite materials can improve the conductivity and increase the active sites to a certain extent. However, the distribution of components in the composite obtained by these methods is random, and also it is difficult to achieve accurate control of the microstructure of composite materials. Therefore, an accurate structural regulation strategy is urgently needed to achieve molecular-level assembly of specific functional units.

Supramolecular chemistry is an interdisciplinary subject involving organic chemistry, material chemistry, and biochemistry. Supramolecular systems are formed through reversible non-covalent bonds (such as hydrogen bonds, electrostatic interactions, halogen bonds, ionic dipoles, and π–π interactions) between several chemical species molecules, which are a high complexity chemical system with certain organization.[35–37] It is indispensable to assemble molecular modules through non-covalent interactions in various solvents or bulk liquid or solid systems for the fabrication of supramolecular materials.[38,39] Different from the rigid bond (molecular covalent bond/ionic bond), a key advantage of supramolecular materials is to assemble a variety of different functional units to form brand-new function materials by using flexible non-covalent bonds.[40,41] These non-covalent reversible bonds allow supramolecular systems to exhibit regeneration/self-healing properties along with structural flexibility and mobility that are highly needed for energy storage devices.[42,43] For example, the challenge of designing materials for energy storage and conversion involves combining multiple components through specific interactions to produce truly functional energy storage materials.[44] Supramolecular bonding (hydrogen/electrostatic interaction) is characterized by its moderate binding energies compared to covalent bonds.[45,46] The moderate bonding strength not only ensures the interaction between the supramolecular solid scaffold and polar solvated electrolyte ions, but also is effective in providing improved ion conductivity in both interface and bulk regions.[47,48] In order to realize the rapid response ability of electrodes in charge–discharge processes, the synergistic interaction between electrode materials and electrolyte ions is essential. Among the many possibilities, supramolecular nanostructured materials are best suited to overcome these challenges. Supramolecular materials can be used as electrode materials as well as electrolytes in supercapacitor systems.[49,50] Supramolecular interactions not only benefit the solid electrolyte (gel) polymer electrolyte, but can effectively improve the ionic conductivity in the electrolyte/electrode interface, which is an onerous challenge for solid-state SCs.[51,52]

By precision-oriented self-assembly of different molecules through non-covalent action, large supramolecular aggregates can be formed, which are also known as "supramolecular polymers". The different components in supramolecular systems are combined at the atomic level, and by using well-designed self-assembly strategies, supramolecular polymers with specific structures can be obtained. In the self-assembly field, a number of systematic methods based on molecular geometry have been developed, such as the Israelachvili rule for surfactants based on molecular shapes.[53] In recent years, supramolecular assembly has been widely used to prepare a series of new materials with complex topological structures, for example, mushroom,[54] twisted ribbon,[55] hairpin,[56] hollow tube,[57] *etc.* The use of supramolecular assembly strategies to obtain energy materials with excellent charge storage and ion transport capabilities is a hot research point in this field. From this perspective, the non-covalent interaction of components in supramolecular systems can be very useful and versatile. This hybrid design method can achieve functional integration that cannot be achieved by other methods.

Considering these merits of supramolecular materials, it can be considered that supramolecular self-assembly strategies have great research value in the fabrication of advanced supercapacitor electrode materials. This review covers recent advances in supramolecular self-assembly strategies for the preparation of state-of-the-art electrode materials and electrolytes in supercapacitors. Several examples are presented to discuss the strategic concepts of supramolecular self-assembly for the precise structural design, chemical synthesis, and self-assembly of high-performance carbon materials, metal oxide materials, and conductive polymer materials. Meanwhile, the key design concepts of supramolecular self-assembly for the development of integrated functional electrode materials in a multi-component system are summarized from a comprehensive case study. We hope that this review will help transfer knowledge from reported studies and provide new ideas for the

application and development of supramolecular self-assembly in electrode materials for supercapacitors.

2. Supramolecular self-assembly method for the preparation of advanced supercapacitor electrode materials

2.1 Carbon-based materials

Carbon-based materials with their high surface area, diverse low-dimensional morphology, and exceptional physical and chemical stability have long been the go-to electrode materials for supercapacitors.[58] The family of carbon materials includes graphite, porous activated carbon,[59] carbon aerogel,[60,61] graphene,[62] carbon nanotubes,[63,64] *etc*. Carbon-based materials usually have good electrical conductivity and excellent chemical stability, which makes them exhibit good high current charge–discharge performance and cycle stability. Compared with pseudocapacitor materials, the theoretical specific capacity of carbon materials is lower (usually several hundred F g^{-1}). Although there has been a lot of progress in the structural morphology research of carbon-based materials, the large porosity curvature, lack of pseudocapacitive effect, and tendency to aggregate of carbon-based materials can result in low practical capacitance. To address these shortcomings, two approaches have been developed: (1) preparing porous carbon with well-defined porous structures and controllable pore sizes through precise structural regulation strategies, for example, by controlling the precursor structure to obtain pore sizes that match electrolyte ions and improve charge storage capacity; and (2) doping heteroatoms into the structure of carbon materials to induce additional pseudocapacitive active sites and enhance the surface wettability. This paper mainly introduces the application of supramolecular self-assembly strategies in structure regulation and heteroatom doping of carbon-based materials.

2.1.1 Structural regulation of carbon materials. Hierarchical porous carbons (HPCs), which contain micropores, mesopores, and macropores, have become a focus of research within the carbon family. In HPCs micropores provide the main adsorption sites, while mesopores and macropores facilitate effective material transport.[65,66] Current researchers are primarily focused on controlling the pore size distribution, volume fraction of pores, and morphology of HPCs, while improving energy density, power density is taken into account.[67–69] A recent theoretical study has illuminated that not all hierarchical pores are equally valuable, and the connectivity between pores has a profound effect on electrochemical charge. A well-connected pore structure promotes electrolyte transport, while isolated pores are difficult to access, especially at high current density.[70] The most common method for preparing porous carbon is physical/chemical activation of organic precursors.[71,72] However, this method typically results in a high surface area but limited ability to regulate pore structure and a random pore size distribution. By using supramolecular polymers as soft templates and carbon sources, the pore structure of HPCs can be controlled by the molecular structure of the template after carbonization. Since supramolecular aggregates have a relatively ordered structure, this method can achieve accurate regulation of pore structure.

Yao's[73] group prepared a γ-CD/F127 complex by inserting epoxy-polypropylene (PPO) chains of PEO-PO-PEO (F127) into the hydrophobic cavity of γ-CD through host–guest interaction *via* hydrophobic attraction. The γ-CD/F127 supramolecular complex then self-assembled into mono-micelles. In further hydrothermal treatment process free γ-CDs and γ-CD/F127 supramolecular complex further combined to form larger spheres. After high temperature carbonization and KOH activation of the supramolecular complex, the free γ-CDs on the outer and inner of the polymer formed a large carbon sphere skeleton, while the γ-CD/F127 mono-micelles transformed into carbon quantum dots with a pore diameter of 10 nm. This resulted in a unique ball-in-ball structured HPC-NS with a large specific surface area (765 m^2 g^{-1}). Fig. 1a shows the formation mechanism for HPC-NS, where nanopores in macrospheres are interconnected on scales below 10 nm – the lowest pore separation ever reported.[73] Good pore connectivity can significantly enhance electrolyte transport in the pore network. The HPC-NS obtained by this method exhibited high specific capacity (405 F g^{-1} at 1 A g^{-1} and 71% capacitance retained at 200 A g^{-1}), a wide voltage window (up to 1.6 V in aqueous electrolyte), and high energy as well as power density.[73] Additionally, this work developed a method for evaluating pore connectivity, where the size of the main units constituting interconnected 3D-Hpcs, the longest possible pore separation (LPPS), can be used to characterize pore profiling and serve as a guide for designing high-performance HPCs. Cucurbit[6]uril (CB [6]) is a pumpkin-shaped supramolecule with a 5.8 A diameter cavity that can be used as a carbon source to prepare narrowly dispersed subnano/mesoporous materials. Cui[74] *et al.* obtained a CB[6] supramolecular complex (SPCC) by selective coordination of the CB[6] and Ba^{2+}. As shown in Fig. 1b the SPCC was post-processed by calcination under an inert atmosphere at high temperature. During the self-pyrolysis process and subsequent washing, the top bond of CB [6] was broken and the cavity opened, leaving a large number of subnano pore cavities in the cucurbit[6]uril carbon materials (CBC-Xs). At the same time, the inner $BaCl_2$ nanocrystals were washed away, resulting in mesoporous and interstitial space in the CBC-Xs. Finally, carbon materials (SCSCS) with subnano/mesoporous structures concentrated in ~5.9 A were obtained. The formation process and pore size distribution of the porous structure can be controlled by adjusting the temperature of the self-pyrolysis process.[74] The centrally distributed pore size of subnanometer-pores in CBC-Xs can smartly match the positive/anion diameter (5.8/2.3 A) of the pure ionic liquid 1-methyl-3-methylimidazolium tetrafluoroborate (MMIMBF4), and the mesoporous pores can provide rapid ion migration channels. As a result, using SCSC as an electrode material in an ionic liquid electrolyte can achieve state-of-the-art performance with a maximum energy density of 117.1 W h kg^{-1}.[74] Graphene has very high theoretical surface and electron transport properties, and can reach a theoretical specific capacitance of 550 F g^{-1}.[75]

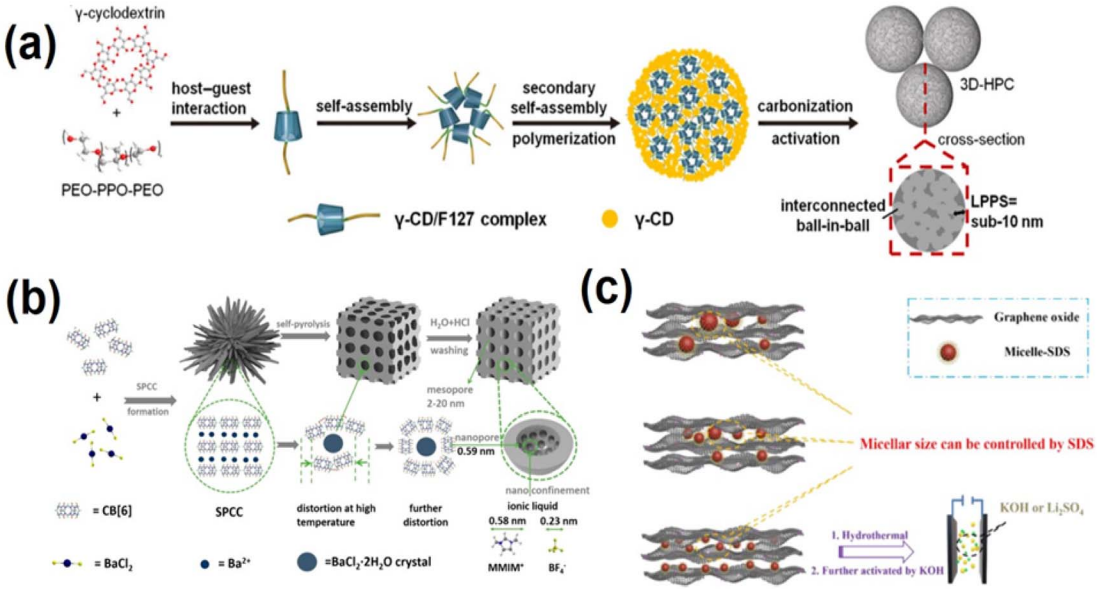

Fig. 1 (a) Illustration of the formation mechanism for HPC-NS with a low longest possible pore separation (LPPS) (high interpore connectivity).[73] Copyright 2022, Wiley-VCH. (b) Formation and the following self-pyrolysis of SPCC at high temperature that creates both mesopores and subnanopores in the resulting carbon.[74] Copyright 2020, American Chemical Society. (c) Schematic illustration of the MGPC-based symmetric supercapacitors and the supramolecular interactions between GO and macromolecule protein micelles.[77] Copyright 2020, Elsevier.

However, interlayer van der Waals forces cause graphene sheets to inevitably restack and overlap, greatly reducing their electrochemical properties.[76] By using graphene oxide (GO) as a precursor, three-dimensional (3D) graphene with the inherent properties of two-dimensional graphene sheets and porous structure can be obtained by the bottom-up method. Chen *et al.*[77] selected milk as a multifunctional biomass additive, using macromolecular protein emulsions (MPMs) in milk as a pillaring agent. The supramolecular interaction between MPMs and GO effectively prevents reaccumulation and overlap of GO sheets (the synthesis mechanism is shown in Fig. 3c). The size of the MPMs can be adjusted by controlling the concentration of sodium dodecyl sulfate surfactant, thus making the surface area and chemical properties of the synthetic Milk/rGO aerogel adjustable. Nitrogen atoms in MPMs can be doped into GO aerogel efficiently and selectively. After the aerogels were processed, porous hybrid nanocarbon materials (MGPC) were obtained through further graphitization and activation of the Milk/rGO aerogel at 600 °C. This material exhibits excellent supercapacitor performance, with a specific capacitance of up to 518.8 F g^{-1} at 0.1 A g^{-1} in 6 M KOH solution. Symmetric supercapacitors with MCP-5 as the electrode show good cycle stability, with the highest energy density reaching 36.7 W h kg^{-1} in the aqueous Li_2SO_4 electrolyte.[77]

2.1.2. Heteroatom doping of carbon-based materials

Heteroatom doping has been shown to be an effective way for enhancing the electrochemical activity of carbon-based materials.[78,79] Among these heteroatoms, nitrogen (N) element is the most widely studied due to its ease of doping and the resulting nitrogen-doped carbon has good electrical conductivity, surface wettability and excellent electrochemical performance.[80–82] Nitrogen-doped carbon materials can be obtained by using N-containing organic supramolecular polymers as precursors or assembling N-containing supramolecular polymers with a carbon source.[83–85] Melamine-cyanuric acid (MCA), a hydrogen bond supramolecular polymer with high nitrogen content, rich functional groups (–NH_2 and –COOH), variable morphology and easy decomposition characteristics, can be used as the ideal nitrogen source.[86,87] Liu's group used MCA as the template growth agent and nitrogen source; in the presence of glucose, MCA was restructured and an MCA/C aerogel with a one-dimensional rod-like structure was obtained (Fig. 2a).[60] Nitrogen-doped nanotube carbon aerogel (N-NTC) was obtained *via* high temperature carbonization of the MCA/C aerogel. The prepared N-NTC aerogel has a unique one-dimensional nanotube-like structure, high nitrogen content, extremely high specific surface area, large inner diameter and uniform wall thickness. This work systematically analyzed the formation mechanism of the N-NTC aerogel and comprehensively studied the effect of carbonization temperature on the morphology structure and chemical properties of the N-NTC aerogel. When used as an electrode material for supercapacitors (SCs), the N-NTC aerogel exhibited a specific capacitance of 563 F g^{-1} at 1 A g^{-1}. The corresponding symmetric SC devices exhibit a high energy density of 21 W h kg^{-1}.[60] In our previous work,[88] melamine-cyanurate supramolecular polymers were connected to –COOH and OH on GO surface by non-covalent bonding force to generate a GO/melamine cyanurate (GO/MC) supramolecular system (Fig. 2b). GO/MC was then hydrothermally treated and calcined at 350 °C to obtain nitrogen-doped graphene with a porous structure and nitrogen doping content up to 10.5%. The introduction of the MC supramolecular polymer acts as

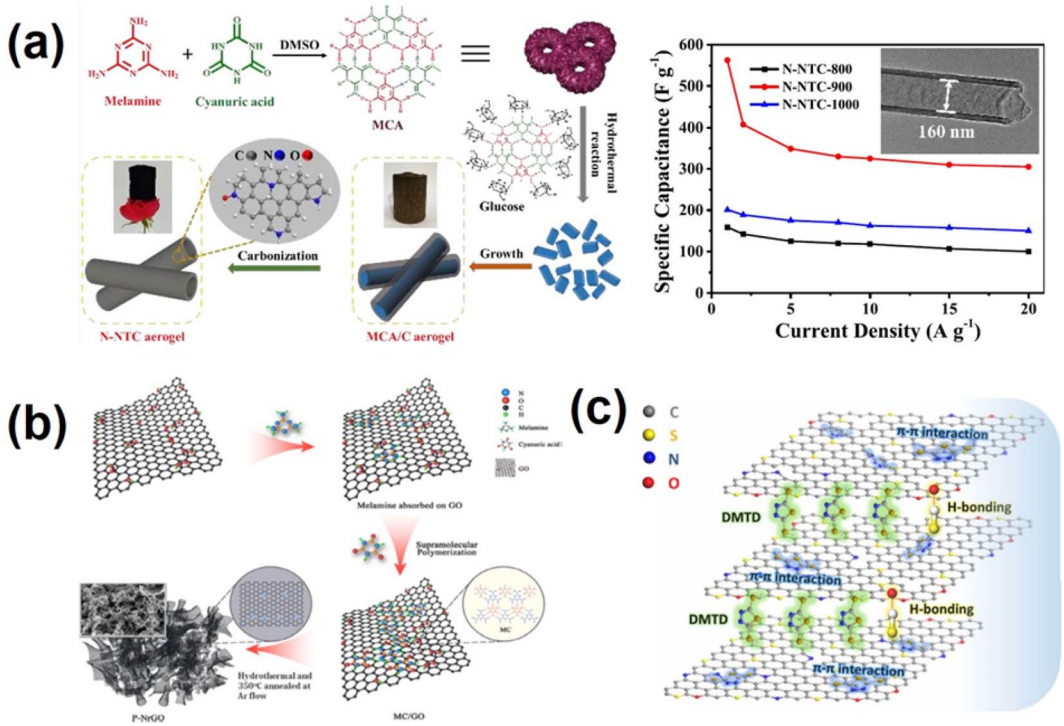

Fig. 2 (a) Schematic illustration of the synthesis and rate performance of the N-NTC aerogel.[60] Copyright 2021, American Chemical Society. (b) Schematic illustration of the supramolecular polymerization method for preparing P-NrGO materials.[88] Copyright 2018, Elsevier. (c) Schematic illustration of the interactions between GO and DMTD molecules.[91] Copyright 2020, Elsevier.

a barrier to prevent overlapping of graphene sheets, while also serving as a soft template for pore-making and *in situ* nitrogen doping. The nitrogen doping level and pore structure of the final product can be manipulated by controlling the relative ratio of GO to MC. The obtained P-NrGO showed a specific capacitance of 355 F g^{-1} at 1 A g^{-1}, and possessed excellent cycling stability.[88] In a similar way, we also carried out supramolecular self-assembly of a melamine-phytic acid (MP) supramolecular polymer,[89] which contains nitrogen and phosphorus atoms, with GO to obtain a GO/MP supramolecular system, and further calcined it at high temperature to obtain porous N, P co-doped graphene. L-cysteine is a kind of amino acid containing nitrogen and sulfur elements. L-cysteine molecules were grafted onto the oxygen-containing functional group of GO through supramolecular interaction, followed by hydrothermal and high-temperature treatment to obtain N and S co-doped graphene with excellent supercapacitor performance.[90] Zhang *et al.*[91] applied 2, 5-dimercapto-1, 3, 4-thiadiazole (DMTD) as a bifunctional pillared agent and efficient dopant precursor. Fig. 2c illustrates that the planar DMTD molecules were assembled with graphene oxide (GO) through strong supramolecular π–π and hydrogen bond interactions to prevent reaccumulation of graphene sheets. The amount and efficiency of doping are enhanced, which is conducive to improving the performance of the sandwich-like N, S co-doped three-dimensional (3D) porous graphene aerogels (NSGAs).[91] To sum up, the molecules or supramolecular polymers containing specific heteroatoms can be combined with amphiphilic GO through non-covalent interaction and then post-treated through processes such as hydrothermal or high-temperature calcination to obtain the corresponding heteroatom-doped graphene. The biggest advantage of this method is its high doping efficiency, more uniform and stable doping, and mild doping conditions. However, the mechanism of supramolecular combination with GO and structural changes during post-treatment processes are not yet well understood and require further study.

To sum up, carbon-based materials prepared by supramolecular self-assembly strategies have the following characteristics:

(1) The porous carbon-based materials obtained by supramolecular self-assembly strategies possess a highly ordered structure and highly controllable pore size. Since the structure of the supramolecular precursor is relatively ordered, the pore structure of the carbon-based material derived from supramolecular self-assembly is more ordered than that obtained by traditional chemical activation methods. By selecting different supramolecular precursors, carbon materials with a hierarchical porous structure can be obtained, and the pore size can be adjusted according to the size of electrolyte ions, so as to improve the surface utilization of porous carbon and increase its actual capacitance.

(2) The heteroatom doped carbon-based materials obtained by supramolecular self-assembly strategies have uniform heteroatom distribution and adjustable doping state and amount. Through supramolecular self-assembly strategies, the

doping amount of heteroatoms and the morphology of doped carbon materials can be accurately regulated, and the chemical state of doped heteroatoms can be effectively controlled, resulting in higher activity of heteroatom doped materials. The synergistic effect between excellent structure and highly adjustable doping state results in high energy density, good rate performance and excellent cycle stability of supramolecular-derived heteroatom doped carbon-based materials.

2.2 Structure and property regulation of transition metal-based electrode materials

The specific capacitance of transition metal-based electrode materials, such as transition metal oxides,[92] hydroxides[93] and sulfides,[94] is several times higher than that of carbon materials. However, the high resistance and poor structural stability of these pseudocapacitor materials[95,96] result in unsatisfactory rate performance and cycle stability. Coordination supramolecular networks (CSNs) are another type of coordination supramolecular material, in which supramolecular synthons include simple metal–organic complexes (mononuclear, binuclear, *etc.*) or first formed from metal ions/clusters and organic ligands to form oligomerized coordination entities. These entities are then assembled into coordination supramolecular networks through hydrogen bonding, π–π self-stacking, van der Waals interactions, hydrophobic effects, *etc.*[97,98] CSNs not only have the advantage of adjustable pore size or space of MOF materials, but also, contrary to rigid MOF crystals, the weak interaction between supramolecular synthons makes the structure of CSNs more flexible, and the pore size or space of CSNs can be adjusted to match the size of electrolyte ions, and the steric hindrance to ion insertion is greatly reduced.[99,100] However, the preparation of electrodes from powder CSNs requires the addition of insulating polymer binders and conductive additives, which reduce the effective surface area of the CSNs and increase the internal electrode resistance.[101] Therefore, direct growth of CSNs on a conductive collector or conductive material (graphene) with a high specific surface are two ways to address these issues.

The solvothermal method is a common way to achieve *in situ* growth of CSNs on conductive substrates. As illustrated in Fig. 3a Yang's group[102] used Ni foam as both the nickel ion source and current collector. They first reacted the nickel foam with hydrochloric acid to generate nickel ions, and then the salicylic acid ligand and nickel ions were coordinated on the surface of the Ni foam skeleton to form a mononuclear metal–organic complex. Finally, a large number of mononuclear complexes rapidly self-assembled into a submicron array of Ni-salicylic acid CSNs by intermolecular interaction. Zhang's group[103] used the same method, employing Co foam as the Co ion source and substrate and salicylic acid as the ligand, to *in situ* grow a helical rod new cobalt base coordination supramolecular network (Co-CSN) on the Co base. Helical micro- and nano-structured Co-CSN has a three-dimensional (3D) network formed by hydrogen bonding. Fig. 3b reveals the formation of Co-CSN. This *in situ* growth method not only takes full advantage of the pseudo capacitance of the coordination supramolecular network, but also enables close contact with the metal substrate without a binder. The unique submicron rod array structure enlarges the specific surface area, increases the electroactive sites, and reduces the diffusion distance between the electrolyte and electrode. Yang's group[104] used Ni ions as the coordination center, potassium thiocyanate and isonicotinic acid as ligands, and Mn ions as dopants to grow a Mn-doped nickel CSN material on the nickel foam substrate by a simple one-step solvothermal method (Fig. 3c), and investigated the influence of Mn on the morphology, composition, structure and electrochemical properties of Ni-CSN. The Mn-doped binder-free electrode has an extremely high surface capacity. When the current density increases from 10 mA cm^{-2} to 50 mA cm^{-2}, the capacitance retention rate is 73.33%. Zhang's group[105] first achieved *in situ* growth of Ni coordination supramolecular nanowires (Ni-CSN) on the current collector by using Ni foam as the nickel ion source. Then by suffixation, a free-standing Ni_3S_2 nanowire electrode was successfully obtained. The Ni_3S_2 electrode showed a high specific capacitance of 5.8 F cm^{-2} at 5 mA cm^{-2} due to its structural flexibility and abundant open redox reaction sites. Based on these advantages, the self-supported Co-CSN spiral micro nanorods of the material provide a high areal capacitance of 10.19 F cm^{-2} and good rate performance.

CSNs can be closely self-assembled with carbon-based materials (especially graphene with a large specific surface) through intermolecular forces to form composite materials. This prevents them from easily separating even when charged and discharged at high current densities, improving material conductivity and optimizing electrochemical performance. Yang's research group[96] reported a method for assembling the novel nickel-coordinated supramolecular network $[Ni_2(3,5\text{-}PDC)_2\cdot(H_2O)_8\cdot(H_2O)_2]n$ (labeled as Ni-PDC, 3,5-PDC = 3,5-pyridine dicarboxylic acid) with nitrogen doped graphene (NG) to form an excellent composite electrode material Ni-PDC@NG, which is shown in Fig. 3d. Ni-PDC effectively cooperates with NG to significantly improve the electrochemical performance of SCs. The composite electrode exhibits excellent rate capability, maintaining 53% of the initial capacitance at a high current density of 40 A g^{-1} and excellent cycle life. Using a similar method, Yang's team[106] selected pyridine-2, 3-dicarboxylic acid (H_2-pda) as a ligand and successfully constructed a series of Ni-pda@3D reduced GO materials (Ni-pda@3DrGO) by solvothermal reaction of Ni^{2+} with graphene oxide (GO) in H_2O-DMF solution. In this composite, Ni-pda with a special structure is highly coordinated with high conductivity 3DrGO, enabling full use of the active site of pseudocapacitance. The maximum capacitance that the Ni-CSN@3DrGO sample can provide at a current density of 1 A g^{-1} is 952.85 F g^{-1}.[106]

Polyoxometalates (POMs) are nanomolecular clusters composed of multiple transition metals and oxygen-richness and are potential pseudocapacitor electroactive materials.[107] POMs are prone to rapid multi-electron variable redox reaction and multi-electron and proton transport, meanwhile maintaining their original structure during electrode reactions. However, their water solubility,[108] small surface area, and poor conductivity have hindered their practical application in supercapacitors.[109] Currently, two methods are adopted to

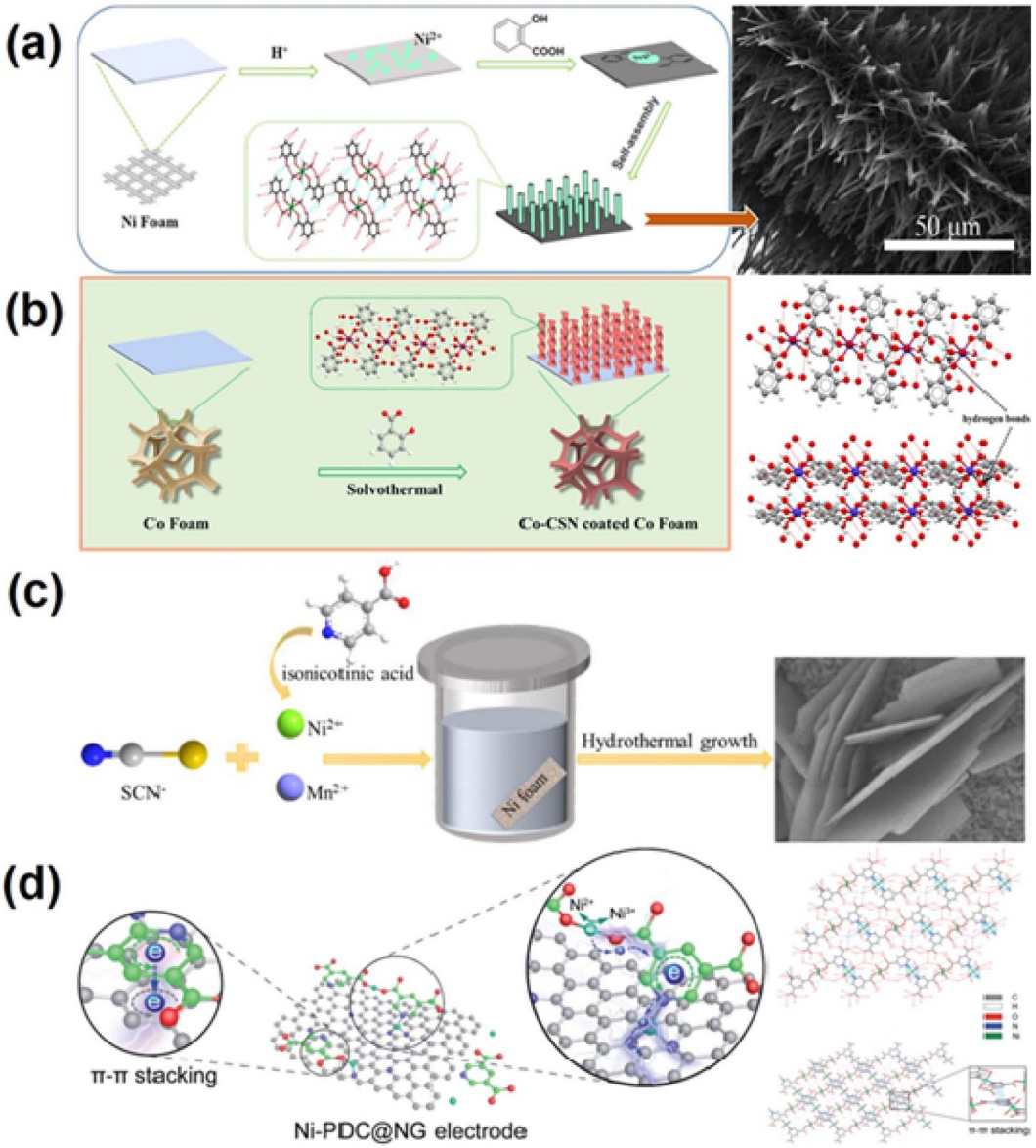

Fig. 3 Coordination supramolecular network derived metal-based electrode materials for supercapacitors. (a) Schematic illustrating the possible formation mechanism and SEM images of the Ni-Hsal CSN electrodes.[102] Copyright 2018, Elsevier. (b) Schematic illustration of the synthetic process of Co-CSN helical micro-nano rods and three-dimensional networks of Co-CSN formed *via* hydrogen bonds.[103] Copyright 2022 Elsevier. (c) The schematic illustration for the fabrication of Mn-NSNA.[104] Copyright 2018, Elsevier. (d) Schematic illustration of the Ni-PDC@NG electrode with continuous electronic conduction pathways and the charge-storage mechanism and the supramolecular network structure of Ni-PDC.[96] Copyright 2017 The Royal Society of Chemistry.

improve the electrochemical performance of POM materials. One approach is to immobilize POMs on appropriate large surface area substrates, such as graphene,[110] porous activated carbon,[111] carbon nanotubes,[112] conductive polymers,[113,114] *etc.* Attaching POMs to highly dispersed substrate materials is challenging due to electrostatic repulsion. Previous studies commonly introduced linkers[115,116] to provide an integrated or tailored scaffold to capture POM molecules. However, POM-based supercapacitors still exhibit low energy density due to poor connectivity caused by blocked interaction and/or decreased interfacial surface area due to the agglomeration of POMs.[116] The key to solving this problem is to improve the dispersion of POM molecules on the substrate, exposing sufficient electrochemical active sites at the molecular level. By using a supramolecular self-assembly strategy, anchoring single PMO molecules by the traditional chemical method has obvious advantages such as simple preparation process, low cost and high yield. Liu's group reported a supramolecular strategy for confining a single polyoxometalate (POM) cluster precisely in a polypyrrole (PPy) hydrogel-wrapped CNT framework with molecular-scale cages.[117] As shown in Fig. 4a, a "fishnet" positively charged PPy hydrogel (TCPP) crosslinking agent doped

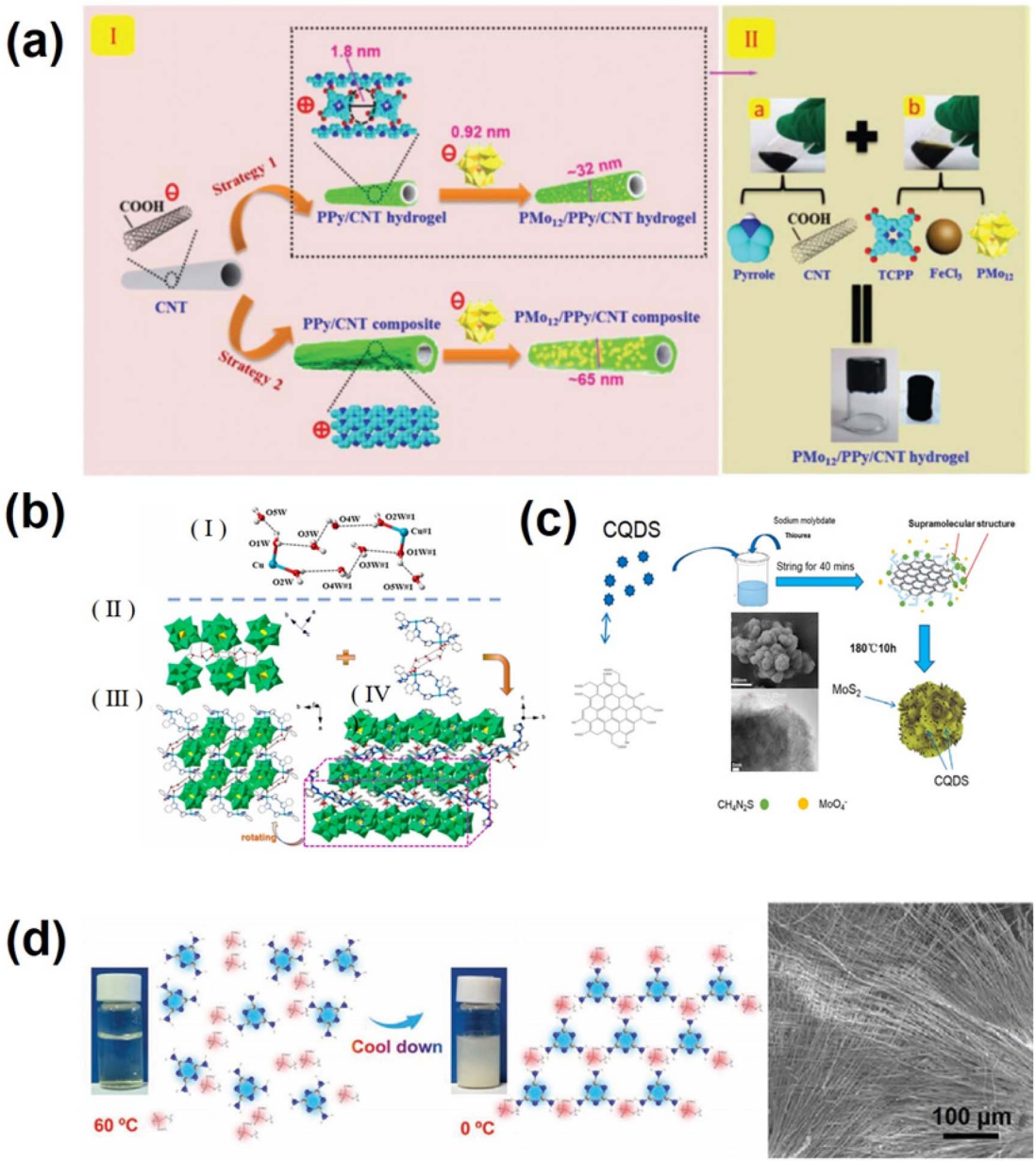

Fig. 4 (a) (I) Electrostatic capture of PMo_{12} molecules by a fishnet-like PPy hydrogel (strategy 1) or blanket-like PPy chain (strategy 2)-wrapped CNT. (II) Fabrication process of the PMo_{12}/PPy/CNT ternary hybrid hydrogel. (Inset) Photographs of the PMo_{12}/PPy/CNT hybrid hydrogel.[117] Copyright 2020 The Royal Society of Chemistry. (b) (I) The view of the chair-shaped water-copper cluster. (II) View of the linkages between water clusters and PMo_{12} POMs. (III) and (IV) Extended PHSF formation view.[123] Copyright 2022, Elsevier. (c) Schematic diagram for the synthesis of MoS_2/NCQDs. Inset: SEM and high resolution TEM of MoS_2/NCQDs-6.[125] Copyright 2022, Elsevier. (d) Synthetic mechanism diagram of V-supramolecular nanoribbons and SEM image of V-supramolecules with the mass ratio of NH_4VO_3 to $C_3H_6N_6$ of 2.8.[127] Copyright 2022 Wiley-VCH.

with 5,10,15,20-tetrad (4-carboxyl) porphyrins uniformly coated the outer surface of negatively charged carbon nanotubes, while creating a cage structure with ~1.8 nm nanopores (DFT calculation). To facilitate the capture of $PMo_{12}O_{40}$ (about 0.92 nm in diameter), the final PMo_{12}/PPy/CNT ternary hybrid hydrogel active material with a single molecule dispersed PMo_{12} was obtained. The "cage" effect also activated the PMo_{12} molecule, enhancing its charging/discharging performance by introducing new proton transfer active sites.[117] The well-structured interconnection network enhanced connectivity and flexibility.[117] The flexible solid supercapacitor with the PMo_{12}/PPy/CNT electrode had a power density of 700 μW cm^{-2} and a high energy density of 67.5 μW h cm^{-2}. Another strategy is to combine POMs with a suitable metal–organic complex (MOC), which not only perfectly overcomes the inherent disadvantages of pure POM electrodes, but also provides additional advantages to the electrode material (including but not limited to an ordered crystal structure, modulated conductivity and rate

properties, and low solubility in water and common organic solvents).[118–121] Additionally, the POM-based MOC electrode material can be obtained by a simple hydrothermal method, and its clear structure facilitates the study of the corresponding relationship between the structure and properties. Hydrogen bond supramolecular scaffolds (HSFs) are a subclass of MOCs. In POM-HSFs, hydrogen bond interactions are important not only in self-assembled supramolecular frameworks but also provide electron transport and/or proton conduction pathways to enhance electrochemical performance.[122] Pang's group[123] prepared two nitrogen-rich organic ligands 1-imidazol-1-ylmethyl-1*H*-benzotriazole (imbta) and 1-pyridine-3-ylmethyl-1*H*-benzotriazole (pybta), and chose three $PMo_{12}O_{40}^{3-}$ Keggin POM, $CuAc_2 \cdot H_2O$ and $AgNO_3$ salts to prepare three novel water cluster enclosed polyoxometalate-based hydrogen bond supramolecular frameworks (PHSFs) $[Cu_2(H_2O)_4H_2(imbta)_4](PMo_{12}O_{40})_2 \cdot 6H_2O$ (1), $Cu(H_2O)_2H_4(pybta)_4(PMo_{12}O_{40})_2 \cdot 2H_2O$ (2), and $[Ag_2H_7(pybta)_6(PMo_{12}O_{40})_3] \cdot 12H_2O$ (3) through a hydrothermal method. The detailed structure of the PHSF is displayed in Fig. 4b. The encapsulation of water clusters into the porous structure of PHSFs improves the conductivity of the electrode material and stabilizes the entire space as a guest. Owing to the unique PHSF structure of (PHSFs) $[Cu_2(H_2O)_4H_2(imbta)_4](PMo_{12}O_{40})_2$ with numerous O–H···O interactions, the maximum specific capacitance of the compound 1-based electrode is 710 F g^{-1} at 1 A g^{-1},[123] which is better than that of most of the reported POM-based electrodes.

MoS_2 features a two-dimensional (2D) layered structure similar to graphene,[124] which exists basically in 2H and 1T crystal phases. Compared to 2H phase MoS_2, 1T phase MoS_2 has superior electrochemical activity and has attracted widespread attention in the fields of electrochemistry and energy storage. However, it is challenging to synthesize 1T MoS_2 by common chemical methods. Shu's group[125] synthesized nitrogen-doped carbon quantum dot modified 1T phase molybdenum disulfide (MoS_2/NCQDs) using a supramolecular assisted method. As shown in Fig. 4c, citric acid was first reacted with urea to form NCQDs. Oxygen containing functional groups (–OH and –COOH) on the surface of the carbon quantum dots can be connected with thiourea through hydrogen bonding to form supramolecular structures.[85] During the hydrothermal process, the thiourea in the supramolecular system combines with sodium molybdate and transforms into MoS_2. The formed supramolecules can also act as intercalators to promote the transition from triangular prismatic 2H-MoS_2 to triangular antiprismatic 1T-MoS_2. As MoS_2 nanosheets grow, the carbon quantum dots in the supramolecular system can be anchored to the MoS_2 nanosheets and further act as intercalation agents to effectively prevent the aggregation of MoS_2 nanosheets.[126] The 1T-2H phase MoS_2 in the resulting MoS_2/NCQD materials features a few layered structure with an ultra-wide space of 0.95 nm, facilitating the diffusion of electrolyte ions. Under the synergistic action of NCQD introduction and the formation of 1T phase MoS_2, the conductivity and hydrophilicity of MoS_2/NCQD materials have been greatly improved, and the prepared MoS_2/NCQDs-6 has excellent supercapacitor performance (379.5 F g^{-1} at 0.5 A g^{-1}) and excellent magnification performance (269.7 F g^{-1} at 10 A g^{-1}).[126]

Vanadium supramolecules (V-supramolecules) and their derivatives are in great demand due to their potential applications in various fields, especially as the electrode for supercapacitors and batteries.[127] However, studies on V-supramolecules are still lacking, and there are many shortcomings: (1) the metal centers of V-supramolecules are mainly vanadium trichloride (VCl_3), tetravalent vanadium sulfate (IV) hydrate ($VO_SO_4 \cdot nH_2O$), vanadium dioxide (VO_2) and vanadium chloride (VCl_4), and the prices of these metal centers are relatively expensive. (2) The preparation of vanadium MSPs is a complex, time-consuming and lengthy process; (3) due to the complex synthesis process (high temperature and pressure), key issues related to the nucleation and growth of vanadium MSPs remain unresolved. To address these problems, the $C_3H_6N_6$–NH_4VO_3 supramolecular (V-supramolecular) nanoribbons (Fig. 4d)[127] with an "aloe vera" shape using cheap and readily available NH_4VO_3 as the vanadium metal center and $C_3H_6N_6$ as the organic ligand were fabricated through a rapid cooling self-assembly method by pang *et al.*[118] The highlight of this work is that the nucleation and growth mechanism of V-supramolecules were observed *in situ*, and the influences of precipitation temperature, cooling rate, stirring and drying methods on nucleation and growth were analyzed. The VN/C nanoribbons derived from $C_3H_6N_6$–NH_4VO_3 supramolecules possess high specific capacity. Different from conventional methods, this method is simple, efficient and suitable for large-scale preparation.

2.3 Structure and property regulation of conducting polymers

Conductive polymers (such as polyaniline, polypyrrole, *etc.*) possess high conductivity, good flexibility, low cost, and extremely high theoretical capacitance. However, the poor electrochemical stability limits their practical application in supercapacitors, making it urgent to improve the cycling stability of conductive polymer materials.[128–130] To date, two main strategies have been used to improve polymer cycling performance: (1) nanocomposite strategy (solution blending and *in situ* growth method). However, the improvement of the cycling performance by the nanocomposite strategy is limited due to the drawbacks such as mechanical expansion during ion insertion and delamination of electrode materials from substrates. Through the precise supramolecular self-assembly strategy, the morphology of conductive polymer nanocomposites can be effectively regulated, the connection between the conductive polymer and substrate can be strengthened, and the molecular dispersion of the conductive polymer on the substrates can be realized. Kuila's group[131] reported a simple but efficient route based on the supramolecular approach for large scale synthesis of intercalated polyaniline graphene nanohybrids with three dimensional pillar structures. First, GO was linked with pyrene butyric acid (PBA) in an alkaline medium by supramolecular forces. Then aniline monomers were protonated by PBA; meanwhile, the interfacial

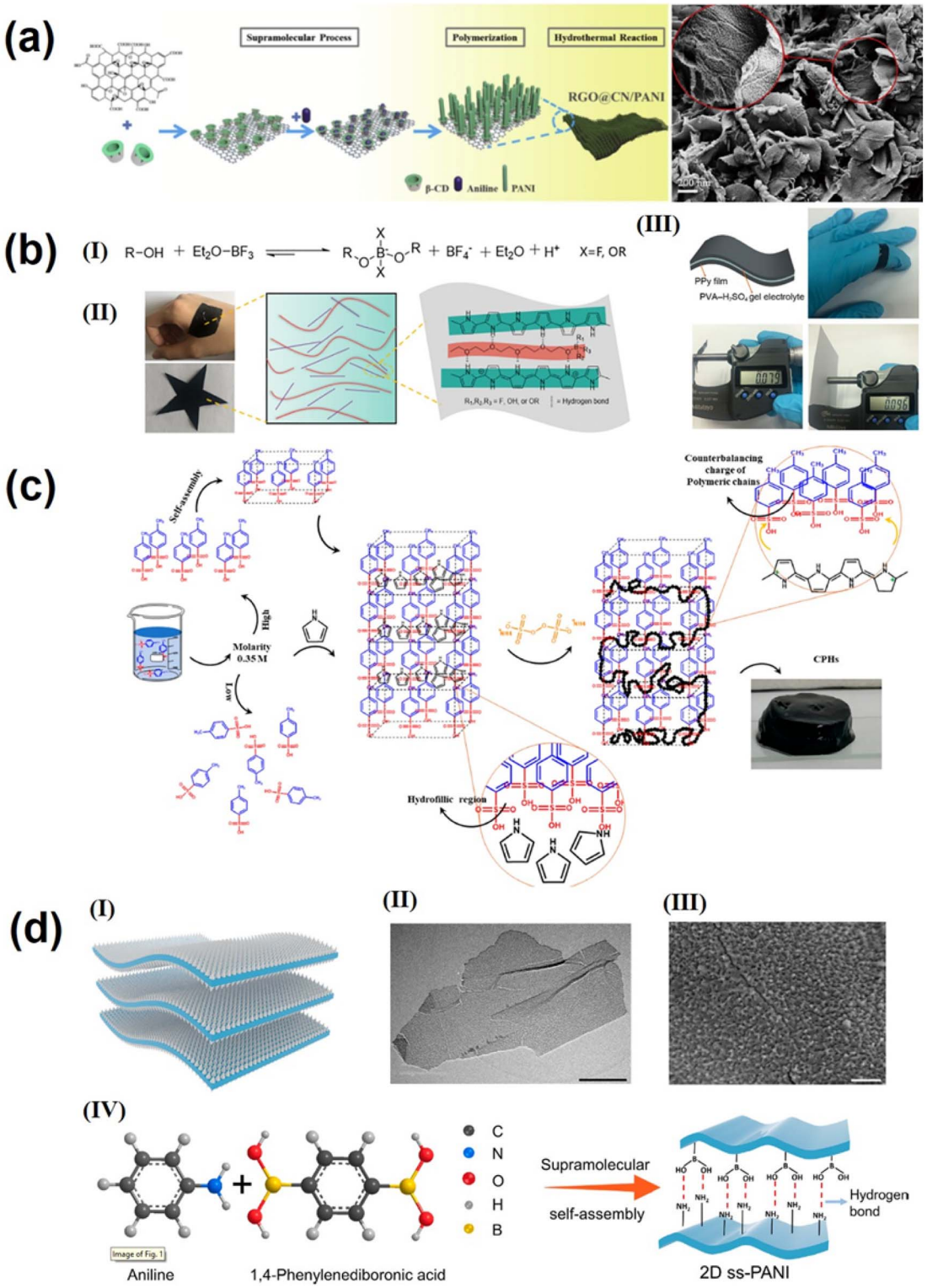

Fig. 5 (a) Fabrication process and SEM image of RGO@CN/PANI nanocomposites.[132] Copyright 2018 Elsevier. (b) (I) Formation of the dynamic PEG-borate polymers possessing negative charges. (II) Photograph of PEG600-PPy films and the dynamic network constructed by rigid PPy chains and soft PEG chains through electrostatic interactions and hydrogen bonds. (III) Schematic illustration and photograph of the UF-SC.[138] Copyright 2020 Elsevier. (c) Schematic representation of PPy-CPH synthesis and hydrogel formation.[139] Copyright 2021 American Chemical Society. (d) A supramolecular assembling strategy to construct ss-PANI nanosheets. (a) Schematic illustration of the structure of 2D ss-PANI. (II) TEM and (III) SEM (the scale bars of II and III are 2 μm and 200 nm, respectively). (IV) Supramolecular crosslinking of aniline with 1,4-PDBA to synthesize 2D ss-PANI consisting of numerous hydrogen bonds.[128] Copyright 2021 Elsevier.

polymerization of aniline monomers (chloroform, water interface) was performed in the presence of an oxidizer. During interfacial polymerization, the protonated aniline monomer attached to the graphene surface acts as an initiator and the polymer grows between the graphene interlayer, and after PBA is removed a porous and pillar polyaniline intercalation reduced graphene oxide structure (PANIRGO) is formed. This three-dimensional porous structure can increase electrolyte penetration and thus improve the utilization of the electrode surface. The PANIRGO material exhibits an optimal capacitance value with good electrochemical stability.[131] A similar supramolecular self-assembly strategy was used in our previous research study,[132] which is shown in Fig. 5a; by supramolecular interaction, β-cyclodextrin (b-CD) was attached to the GO surface, and the hydrophobic inner cavity of β-cyclodextrin was included with polyaniline monomer, inducing *in situ* polymerization of aniline on the GO surface; after hydrothermal treatment, β-CD was carbonized into carbon nanodots anchored on the surface of RGO, and the reduced GO/carbon nanodot/polyaniline (RGO@CN/PANI) nanocomposites presented a regular polyaniline particle array morphology on the surface of the graphene layer. The specific capacitance of RGO@CN/PANI nanocomposites is up to 871.8 F g^{-1} at a current density of 0.2 A g^{-1} and has good cycle performance.[132]

Conducting polymer hydrogels (CPHs), such as poly(3,4-ethylene dioxythiophene) (PEDOT), polypyrrole (PPy) and polyaniline (PANI) hydrogels, have been widely used in flexible supercapacitors.[19,133,134] However, conductive polymer hydrogels generally have shortcomings such as insufficient electron transport abilities and weak mechanical strength; therefore, non-electrochemically active collectors are usually required for mechanical support and to compensate for the lack of mechanical properties and stability of traditional CP materials. However, the existence of these collectors reduces the overall energy density of flexible capacitors.[135] Inspired by the dynamic network structure of animal dermis, composed of collagen fibrils (rigid and strong) and elastin fibers (soft and elastic), combining a rigid conductive polymer and soft hydrophilic polymer through appropriate supramolecular interaction can produce a high-strength and stable structure of CPHs.[136] This is an effective strategy to construct high strength flexible CPHs. Ma *et al.*[137] used polyvinyl alcohol (PVA) as a soft polymer and polyaniline (PANI) as a rigid polymer, and a polyaniline-polyvinyl alcohol hydrogel (PPH) with a tensile strength of 5.3 MPa (conductivity of 0.1 S cm^{-1}) was formed by cross-linking PVA and PANI with boric acid at the molecular level. Due to the excellent mechanical strength of hydrogels obtained by supramolecular self-assembly, no additional collector is required for structural support. The PVA–PANI hydrogel has excellent capacitive properties (928 F g^{-1}). The energy density of the PVA–PANI hydrogel flexible solid-state supercapacitor reaches 13.6 W h kg^{-1}, and it still has a high capacity retention rate after bending and folding.[137] By the same strategy, the rigid polypyrrole (PPY ∼ 90 wt%) and soft polyethylene glycol (PEG, only 10 wt%) were connected through supramolecular interaction to form a dynamic network structure by Ma's research group (Fig. 5b).[138] The PEG600 obtained by supramolecular crosslinking between PEG (with a molecular weight of 600) and PPy showed the best supercapacitor performance. Compared to the PVA–PANI hydrogel, the PEG600-PPy hydrogel showed a qualitative improvement in tensile strength (92 MPa) and electrical conductivity (110 S cm^{-1}). The high-strength PEG600-PPy hydrogel, therefore, can be used directly as an electrode for the preparation of full polymers without the use of any substrate or current collector. With a thickness of up to 80 μm (thinner than a piece of A4 paper) (Fig. 6b(III)), the fully polymerized flexible supercapacitor provides a large capacity of 547 F cm^{-3} with excellent mechanical and electrochemical stability.[138]

In conclusion, supramolecular self-assembly strategies have significant advantages in the preparation of conductive polymer hybrid materials and conductive polymer hybrid hydrogels. In addition, supramolecular self-assembly strategies can also regulate the conductive properties, morphology and electrochemical properties of monomer conductive polymers at the molecular level. Alcaraz-Espinoza *et al.*[139] used an amphiphilic alkyl sulfonic acid (*p*-toluene sulfonic acid, *p*-TSA), a conventional additive dopant that can improve the electronic conductivity and stability of PPy. When the molar ratio of *p*-TSA to Py monomer was 1, the low water solubility Py monomer was self-assembled by supramolecular self-assembly at the hydrophobic end of *p*-TSA and fully polymerized, forming a micellar structure. It can be observed from Fig. 5c that *p*-TSA has a highly conjugated polymer chain after supramolecular assembly, which not only can improve the overall conductivity, but also can be used as a template to reduce the aggregation and the size of the PPy clusters; PPy has a highly connected 3D network structure and exhibits excellent rate performance and cycle stability as a supercapacitor electrode material.[139] Yang's group[128] used amphiphilic 1,4-phenylenediboronic acid as an additive for supramolecular self-assembly with aniline monomer through electrostatic interaction and hydrogen bonding to form a spherical micelle with 1,4-pdBA outside and aniline inside in solution. With the formation of polyaniline, the spherical micelle was demolished. The growth orientation of PANI was controlled by the hydrogen bond interaction between 1,4-phenylenediboronic acid and PANI, and second superparticle polyaniline (ss-PANI) with a two-dimensional morphology was constructed by the dynamic evolution emulsion polymerization process. Fig. 5d illustrates the structure of 2D ss-PANI; it is indicated that the excellent volume durability and intermolecular hydrogen bonding effect of ss-PANI can effectively inhibit the volume change during repeated charge and discharge. 2D supercapacitors based on ss-PANI have remarkable cycle stability, with a capacitance retention rate of 93.9% over 10 000 cycles.[128]

To sum up, supramolecular materials derived from the supramolecular self-assembly strategy are promising electrode materials for high-performance supercapacitors, because the supramolecular self-assembly strategy can realize the self-assembly of various functional structural units at molecular levels and meet the requirements of electrode materials in different application scenarios. Table 1 summarizes and compares the properties of the three kinds of supramolecular derived electrode materials mentioned above.

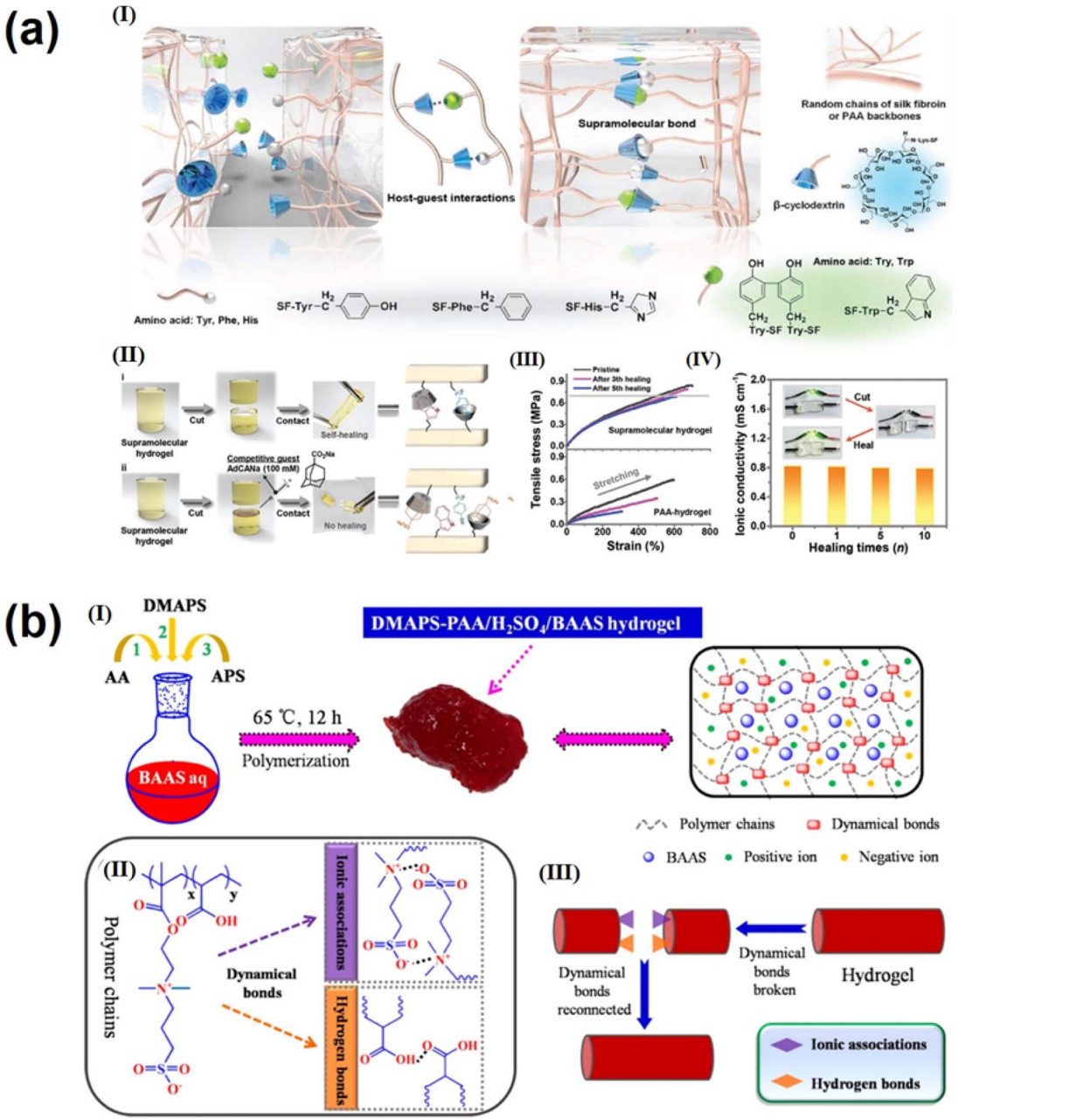

Fig. 6 (a) (I) Schematic diagram of the self-healing mechanism of the supramolecular hydrogels. Supramolecular bonds were formed through host–guest interactions between the grafted β-CD molecules and residual amino acid molecules on the interactive surfaces of the supramolecular hydrogel pieces; (II) self-healing experiments of the supramolecular hydrogels *via* host–guest interactions. (III) Tensile strain–stress profiles of the supramolecular hydrogel and the comparative PAA-hydrogel; (IV) ionic conductivity of the supramolecular hydrogel after multiple times cutting–healing.[148] Copyright 2021 Wiley-VCH. (b) (I) Schematic of the preparation process of the DMAPS–PAA/H_2SO_4/BAAS hydrogel; (II) schematic illustration of the dynamic bonds among the cross-linked polymer chains; (III) schematic of the self-healing mechanism of the hydrogel electrolyte.[149] Copyright 2020 American Chemical Society.

3. Supramolecular self-assembly strategy for the preparation of advanced electrolytes

The electrolyte is one of the key components that affect the performance of supercapacitors. The size of the electrolyte ions, ionic conductivity and mobility, and the wettability of the electrode in the electrolyte have a significant impact on the operating voltage, stability, and energy and power density of the supercapacitor.[144,145] Gel polymer electrolytes (GPEs) with high ionic conductivity, wide voltage windows, good mechanical properties and adequate safety are attracting increasing attention for use in flexible supercapacitors. Next-generation

Table 1 Comprehensive electrochemical performance comparison of three kinds of electrodes materials prepared *via* the supramolecular self-assembly strategy

Electrode Materials	Electrolyte	SC	Cyclic stability	EDLC/PSC	Energy density	Rate capability	OPW (V)	Ref.
N-NTC-900	6 M KOH	563 F g^{-1} (1 A g^{-1})	97% after 10 000 cycles	EDLC&PSC	21 W h kg^{-1}	54.2% (1–20 A g^{-1})	0–1.0	60
HPC-NS	6 M KOH	405 F g^{-1} (1 A g^{-1})	95% after 10 000 cycles	EDLC&PSC	24.3 W h kg^{-1}	33.3% (1–250 A g^{-1})	0–1.2	73
NSGAs-2	6 M KOH	321 F g^{-1} (1 A g^{-1})	92.8% after 6000 cycles	EDLC&PSC	10.52 W h kg^{-1}	80.4% (1–20 A g^{-1})	0–1.0	91
MB@3DrGO	1 M H_2SO_4	311 F g^{-1} (1 A g^{-1})	96% after 10 000 cycles	EDLC&PSC	8.2 W h kg^{-1}	84.2% (1–20 A g^{-1})	0–1.0	140
SPCC	$MMIMBF_4$	233.5 F g^{-1} (0.2 A g^{-1})	95.4% after 20 000 cycles	EDLC&PSC	117.1 W h kg^{-1}	50.5% (0.2–8 A g^{-1})	0–3.8	74
N-MM-Cnets	0.5 M H_2SO_4	537.3 F g^{-1} (0.5 A g^{-1})	98.8% after 10 000 cycles	EDLC&PSC	22.6 W h kg^{-1}	69.1% (1–10 A g^{-1})	0–0.6	84
MGPC-5	6 M KOH	351.4 F g^{-1} (1 A g^{-1})	95% after 5000 cycles	EDLC&PSC	36.7 W h kg^{-1} (in 2 M Li_2SO_4)	71.8% (1–20 A g^{-1})	0–1.6	77
HPNCs-3	1 M H_2SO_4	435.6 F g^{-1} (0.5 A g^{-1})	96.1% after 5000 cycles	EDLC&PSC	—	78.9% (0.5–10 A g^{-1})	0–0.8	80
NS-SHC-8:8	1 M H_2SO_4	258.5 F g^{-1} (0.5 A g^{-1})	94.4% after 20 000 cycles	EDLC&PSC	10.2 W h kg^{-1} (in H_2SO_4/PVA gel electrolyte)	79.9% (0.5–10 A g^{-1})	0–1.0	85
NP-CNC	6 M KOH	435 F g^{-1} (0.05 A g^{-1})	96.1% after 50 000 cycles	EDLC&PSC	130.6 W h·kg^{-1} (as cathode for ZHSC)	71.5% (0.05–50 A g^{-1})	0.2–1.8	83
P-NrGO	6 M KOH	335 F g^{-1} (1 A g^{-1})	94.3% after 10 000 cycles	EDLC&PSC	—	77% (1–5 A g^{-1})	0–1.0	88
NP-rGO	6 M KOH	416 F g^{-1} (1 A g^{-1})	94.6% after 10 000 cycles	EDLC&PSC	22.3 W h kg^{-1}	72.7% (0.5–10 A g^{-1})	0–1.0	89
N/S-rGO	6 M KOH	416 F g^{-1} (0.5 A g^{-1})	110% after 20 000 cycles	EDLC&PSC	—	30% (0.5–5 A g^{-1})	0–1.0	90
PMo_{12}/PPy/CNT hybrid hydrogel	0.5 M H_2SO_4	1170 F g^{-1} (1 A g^{-1})	85.7% after 3000 cycles	PSC	67.5 μW h cm^{-2} solid-state supercapacitor	73.4% (1–5 A g^{-1})	0–1.4	117
Ni-Hsal CSN	4 M KOH	6.04 F cm^{-2} (10 mA cm^{-2})	94% after 15 000 cycles	PSC	2.39 mW h cm^{-3}	76.2% (10–50 mA cm^{-2})	0–1.65	102
$[Cu_2(H_2O)_4H_2(imbta)_4](PMo_{12}O_{40})_2 \cdot 6H_2O$	0.5 M H_2SO_4 + 0.5 M Na_2SO_4	710 F g^{-1} (1 A g^{-1})	91.2% after 1000 cycles	PSC	—	70.2 (1–10 A g^{-1})	−0.2–0.8	123
Ni-PDC@NG	1 M LiOH	735 F g^{-1} (1 A g^{-1})	85.3% after 14 000 cycles	PSC&EDLC	21.7 W h kg^{-1}	53% (1–40 A g^{-1})	0–1.6	96
Ni-pda@3DrGO	1 M LiOH	952.85 F g^{-1} (1 A g^{-1})	97% after 1500 cycles	PSC&EDLC	17.70 W h kg^{-1}	57% (1–10 A g^{-1})	0–1.5	106
Mn-doped CSN	3 M KOH	8.12 C cm^{-2} (10 mA $cm^{-2)}$	90.14% after 4000 cycles	PSC	3.41 mW h cm^{-3}	73.33% (10–50 mA cm^{-2})	0–1.8V	104
Ni_3S_2 nanowires	2 M KOH	5.8 F cm^{-2} (5 mA cm^{-2})	83.7% after 5000 cycles	PSC	2.15 mW h cm^{-3}	50% (5–30 mA cm^{-2})	0–1.7	105
Co-CSN	2 M KOH	10.19F cm^{-2} (3 mA cm^{-2})	84.8% after 10 000 cycles	PSC	2.65 mW h cm^{-3}	76.4% (3–30 mA cm^{-2})	0–1.6	103
3DMoS_2/C@RGO	1 M Na_2SO_4	340 F g^{-1} (1 A g^{-1})	90% after 1000 cycles	EDLC	—	71% (10–100 mV s^{-1})	−0.8–0.2	141
MoS_2/NCQDs	1 M Na_2SO_4	379.5 F g^{-1} (0.5 A g^{-1})	82% after 5000 cycles	PSC&EDLC	33.5 W h kg^{-1}	70.1% (0.5–10 A g^{-1})	0–1.8	125
MoS_2@HCS-17	1 M Na_2SO_4	314.5 F g^{-1} (1 A g^{-1})	87% after 4000 cycles	PSC&EDLC	34.0 W h kg^{-1}	62.3% (1–10 A g^{-1})	0–1.7	124
VN/carbon nanoribbons	6 M KOH	266.3 F g^{-1} (0.5 A g^{-1})	71% after 5000 cycles	PSC&EDLC	25.6 W h kg^{-1}	78.3% (0.5–5 A g^{-1})	0–1.1	127
PPy-CPHs	1 M H_2SO_4	560 F g^{-1} (0.75 A g^{-1})	82% after 5000 cycles	PSC	13 W h kg^{-1}	72% (0.75–10 A g^{-1})	0–0.8	139
PEG600-PPy	1 M H_2SO_4	555 F cm^{-3} (0.5 A cm^{-3})	83% after 2000 cycles	PSC	9.1 mW h cm^{-3}	52.0% (0.3–11 A g^{-1})	0–0.7	138
P-GH	1 M H_2SO_4	292 F g^{-1} (1 A g^{-1})	96% after 10 000 cycles	PSC	10.07 W h kg^{-1}	74% (1–100 A g^{-1})	0–1	142
PANIRGO	1 M H_2SO_4	630 F g^{-1} (0.5 A g^{-1})	81% after 5000 cycles	PSC	—	57.5% (0.5–4 A g^{-1})	−0.2–0.8	131
ss-PANI	PVA/H_2SO_4 gel	378 F g^{-1}	93.9% after 10 000 cycles	PSC	9.93 μW h cm^{-2}	66.7% (0.2–5 A g^{-1})	0–0.8	128
PHMeDOT	10 mM HMeDOT + 0.1 M $LiClO_4$	45.4 ± 0.7 mF cm^{-2} (100 mV s^{-1})	87.5% after 1000 cycles	PSC	—	—	−0.5–1.1	143
RGO@CN/PAN	1 M H_2SO_4	871.8 F g^{-1} (0.2 A g^{-1})	72% after 10 000 cycles	PSC&EDLC	—	76.8% (0.2–10 A g^{-1})	−0.7–0.3	132
PANI–PVA hydrogel	1 M H_2SO_4	928 F g^{-1} (0.5 A g^{-1})	90% after 1000 cycles	PSC	13.6 W h kg^{-1}	84% (1–10 A g^{-1})	0–0.8	137

portable and wearable energy storage devices are often subjected to different mechanical strains and damage; as a result, GPEs with good self-healing properties and excellent tensile and electrochemical properties are essential for realizing advanced flexible wearable supercapacitors. The self-healing properties of traditional gels are achieved through reversible interaction of dynamic covalent and non-covalent bonds, and this involuntary self-healing property severely hinders their application.[146,147] In contrast, supramolecular hydrogel electrolytes are formed through non-covalent interactions such as hydrogen bonding, electrostatic interaction and π–π interactions. These electrolytes have several advantages over traditional gel electrolytes, including the absence of initiators or chemical crosslinking agents, environmental friendliness, easy formation and a simple preparation process. Since non-covalent bonds require only a lower energy to form and break, they have excellent reversibility and self-healing properties; this non-covalent design strategy can be applied to GPEs to enable them to self-heal under mild conditions without significant loss of mechanical and electrochemical properties. Considering the high stress of traditional three-layer supercapacitors under mechanical bending, irreversible structural damage can be caused, including interlayer slip, crease formation, and layering of the electrode–electrolyte interface. Wei's group fabricated an all-polymeric, all-elastic and non-laminated supercapacitor with high mechanical reliability and excellent electrochemical performance by *in situ* integrating a polypyrrole electrode layer into a silk fibroin-based elastic supramolecular hydrogel film with a broad range of hydrogen and covalent bonds.[148] The non-laminated structure of the integrated device avoids slip and delamination between interlayer, while the elasticity prevents crease formation. The supramolecular design of the host–guest interaction in the hydrogel matrix (Fig. 6a(I)) ensures that the self-healing efficiency of the supercapacitor remains close to ≈95.8% even after 30 cut/healing cycles and above 85.2% even after 5 cut/healing cycles at −20 °C (Fig. 6a(II–IV)), reaching the highest level available for foldable flexible supercapacitors. Feng *et al.*[149] prepared a stretchable, self-healing, adhesive, redox-active multifunctional supramolecular hydrogel (DMAPS-PAA/H_2SO_4/BAAS) by free radical copolymerization. In H_2SO_4 aqueous solution containing BAAS, DMAPS and PAA were physically cross-linked through dynamic bonds between polymer chains using APS as an initiator. These bonds included hydrogen bonds between carbonyl and hydroxyl groups and ion association between sulfonic acid and quaternary ammonium groups. The supramolecular interaction is shown in Fig. 6b;[149] in addition, the supramolecular hydrogel showed good self-adhesion on the electrode, preventing relative displacement and delamination between the electrolyte and electrode layer during repeated mechanical deformation and facilitating the lightweight and portability of energy storage devices. In addition, BAAS is introduced as a redox additive to increase the additional pseudocapacitance in this work. Carbon-based supercapacitors with DMAPS–PAA/H_2SO_4/BAAS hydrogel electrolytes have a specific capacitance of up to 240 F g^{-1}. At the same time, good self-healing ability (Fig. 6b(III)) can withstand more than 400 bends/releases and still retain 96% of the initial specific capacity. In addition, there are many supramolecular gel electrolytes, such as PVA-TA-H_3PO_4 supramolecular gel electrolyte,[51] and PANI-decorated PVA/PHEA;[52] both demonstrated excellent mechanical stability and self-healing. For example, good self-healing ability can withstand more than 400 bends/releases while still retaining 96% of the initial specific capacity.

There are three main types of electrolytes used for supercapacitors: aqueous-based, organic and ionic liquid electrolytes.[150,151] Among these, aqueous electrolytes have attracted much attention due to their high ionic conductivity, low cost, high safety and simple equipment manufacture and operation.[152,153] However, the low working potential window (usually around 1.00 V) and narrow working temperature range (0–100 °C) are the two major drawbacks. The use of "water-in-salt" (WIS) electrolytes, such as LiTFSI, can effectively widen the potential window and reduce the operating temperature of energy storage devices. However, the performance of WIS electrolytes decreases rapidly at high temperatures because organic solvents in the electrolyte will inevitably weaken the coordination structure between metal cations and water molecules at high temperatures. Li's group[154] developed a new electrolyte of lithium bis(trifluoromethanesulfonyl) imide (LiTFSI) in a dimethyl sulfoxide (DMSO) and water co-solvent system. Through supramolecular interactions (mainly hydrogen bonding and electrostatic) between LiTFSI, DMSO and water (Fig. 7a(I)), the coordination structure of LiTFSI, DMSO and water in the electrolyte can be adjusted to affect the anion pair of H_2O, electron density and the reactivity of H atom in the electrolyte. This allows for adjustment of the electrochemical stability window of freezing and volatilization of the electrolyte. The supercapacitor assembled with this new electrolyte has an operating voltage of 2.40 V(Fig. 7a(II)) and an operating temperature range up to 130 °C (−40 to 90 °C) (Fig. 7a(III)). Due to the increase of the operating voltage, the energy density of the assembled supercapacitor (21 W h kg^{-1}) is much higher than that of the conventional water-based supercapacitor (10 W h kg^{-1}).[154]

Zinc ion hybrid supercapacitors (ZIHSs) have the advantages of standard electric potential low (0.76 V *vs.* SHE), high theoretical capacity (820 mA h g^{-1}), abundant natural resources, double electron transfer reaction, low toxicity in the aqueous solution and inherent safety.[155,156] However, ZIHSs still face several challenges, such as the energy density of commonly used activated carbon electrode materials being suboptimal and uncontrolled growth of zinc dendrites leading to poor cycling stability.[157,158] Supramolecular gel polymer electrolytes (GPEs) are ideal zinc ionic electrolytes due to their similar ionic liquid conductivity and solid like mechanical properties, friendly environment, easy formation and simple preparation process. In order to inhibit the growth of zinc dendrites and improve the energy density of zinc-ion capacitors, Zhang el ta.[159] developed a new type of Zn^{2+} containing supramolecular gel polymer electrolyte (SGPE) by the classic freeze/thawing method and the simple soaking process; Fig. 7b(I) illustrates the preparation of SGPEs. The optimized SGPE has good mechanical properties and high Zn^{2+} conductivity (89.7 mS cm^{-1}) due to the

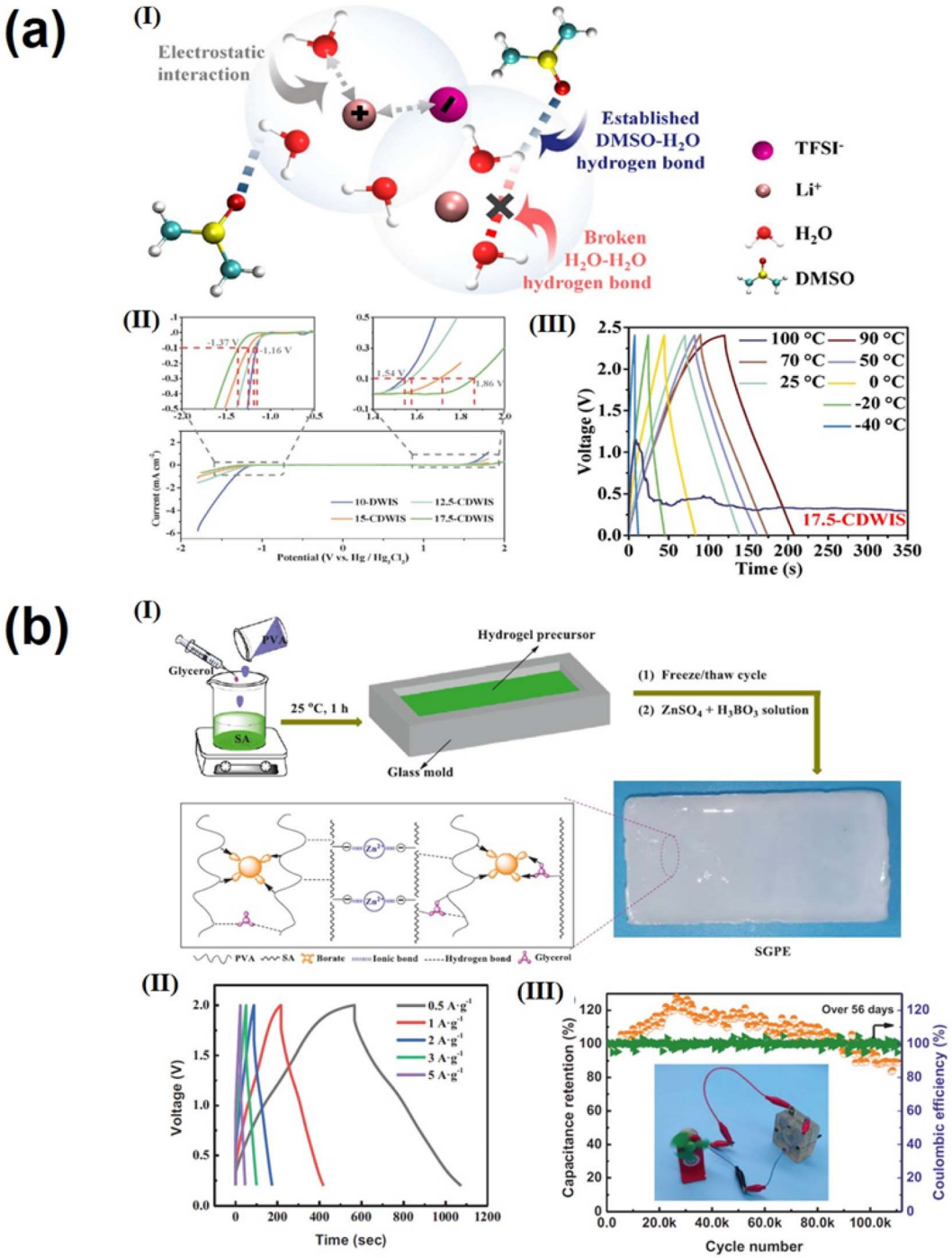

Fig. 7 (a) (I) Schematic illustration of the possible supramolecular interactions among LITFSI, DMSO, and water; (II) electrochemical stability windows of 10-DWIS and X-CDWIS at 10 mV s^{-1}; (III) the GCD curves of SCs with 17.5-CDWIS at 1 A g^{-1} under different operating temperatures.[154] Copyright 2021 Elsevier. (b) (I) Schematic illustration of preparing SGPEs; (II) GCD curves at different current densities of ZIHSs using SGPE-3; (III) cycling performance and coulombic efficiency at a current density of 5 A g^{-1} (digital photo of a mini-fan driven by a ZIHS).[159] Copyright 2022 Elsevier.

interweaving of hydrogen and ionic bond networks. ZIHSs assembled with a SGPE as the electrolyte exhibit a wide voltage window of 0.2–2 V. Due to the inhibition of zinc dendrite growth in SGPEs, the capacitance retention rate is ~84% after 110 000 cycles at 5 A g^{-1}, showing unprecedented cycle durability.[159]

4. Conclusion and perspectives

As the world moves towards renewable and sustainable energy sources, there is an increasing urgency to integrate energy storage devices with high energy density, excellent cycle stability

and mechanical flexibility. The supramolecular self-assembly strategy can realize accurately self-assembly of various functional units at the molecular level using non-covalent bonds. The flexibility and maneuverability of non-covalent bonds between different groups enable the supramolecular self-assembly strategy to produce materials with unique self-healing properties, which are particularly important for energy-related applications. Despite significant progress in the field of supramolecular energy materials, several challenges remain when designing supramolecular materials for next-generation high-performance supercapacitors in the future:

(1) The high cost of supramolecular derived carbon materials: compared to traditional activated carbon, the cost of raw materials used in the preparation of hierarchical porous carbon materials by the supramolecular self-assembly structure regulation strategy is relatively high, which hindered the application in supercapacitors. Therefore, low-cost supramolecular precursors should be developed to enable large-scale preparation of supramolecular-derived carbon materials.

(2) Improving the electrical conductivity of CSNs remains a challenge: although a variety of coordination supramolecular networks (CSNs) with excellent electrochemical activity can be obtained through the coordination of different metal–organic non-covalent bonds, most CSNs have poor conductivity and are prone to aggregation, which requires the use of conductive additives or conductive substrates to give full play to their supercapacitor performance. Therefore, it is still a challenge in the future to select suitable metal ions and coordination systems to prepare CSN materials with stable dispersion and good conductivity.

(3) The structural stability of conductive polymer materials needs to be further strengthened: conducting polymer supramolecular, including electrode materials and electrolytes, exhibit outstanding electrochemical and mechanical properties. However, their mechanical properties should be improved without sacrificing electrochemical properties and conductivity. At present, the maximum fracture/healing cycle of most conductive polymer supramolecular gel electrolytes is only dozens of times, which is far from the level of practical application. Therefore, improving the structural stability of conductive polymer materials remains a challenge.

(4) Dynamic mechanism of supramolecular structure formation is still indistinct: currently, supramolecular self-assembly is mainly achieved by solvothermal or mixing reactions in solution. Most research focuses on characterizing the formed supramolecular structure, with relatively little attention paid to the dynamic mechanism of supramolecular structure formation. However, understanding this dynamic mechanism can provide strong support for the accurate construction of supramolecular systems. To overcome this challenge, some advanced characterization methods (such as *in situ* characterization techniques) and theoretical calculations are needed.

(5) The relationship between the structure and properties of supramolecular materials needs further study: although the synthesis of supramolecular materials is relatively simple and convenient, most supramolecular materials have poor crystallinity, and contain defects and crystal boundaries, making it difficult to accurately characterize their physical properties. Therefore, exploring the relationship between the structure and properties of supramolecular materials using experimental and theoretical methods such as DFT calculations and molecular dynamics (MD) simulations has become an active field of research.

Most excitingly, supramolecular materials are supported by a large number of structurally diverse molecules that can be assembled together in a variety of ways to form functionally diverse materials, which makes supramolecular materials an important application prospect in the field of energy storage. In summary, further studies are needed on the formation mechanism of supramolecular structures and the relationship between their structures and electrochemical properties. Systematic theoretical guidance on supramolecular self-assembly strategies is still insufficient. Further in-depth and systematic studies on the above challenges and prospects are needed to fill the gap between laboratory research and industrial applications of supramolecular energy materials.

Conflicts of interest

We declare that we have no known competing financial interests or personal relationships that could have appeared to influence the work reported in this paper.

Acknowledgements

The authors are grateful to the following financial support of this work: Key Scientific Research Projects of General Universities in Guangdong Province, Grant Number: 2021KCXTD086; Science and Technology Projects in Guangzhou, grant number: 202204400805; the Quality and Reform Project of Guangdong province undergraduate teaching (No. XQSYS-2222873).

References

1 S. Bashir, K. Hasan, M. Hina, R. Ali Soomro, M. A. Mujtaba, S. Ramesh, K. Ramesh, N. Duraisamy and R. Manikam, *J. Electroanal. Chem.*, 2021, **898**, 115626.
2 Y. Shao, M. F. El-Kady, L. J. Wang, Q. Zhang, Y. Li, H. Wang, M. F. Mousavi and R. B. Kaner, *Chem. Soc. Rev.*, 2015, **44**, 3639–3665.
3 S. Manoharan, P. Pazhamalai, V. K. Mariappan, K. Murugesan, S. Subramanian, K. Krishnamoorthy and S.-J. Kim, *Nano Energy*, 2021, **83**, 105753.
4 P. Xue, C. Guo, L. Li, H. Li, D. Luo, L. Tan and Z. Chen, *Adv. Mater.*, 2022, **34**, 2270109.
5 C. Kim, D. Y. Kang and J. H. Moon, *Nano Energy*, 2018, **53**, 182–188.
6 Y. Zhang, H. Mei, Y. Cao, X. Yan, J. Yan, H. Gao, H. Luo, S. Wang, X. Jia, L. Kachalova, J. Yang, S. Xue, C. Zhou, L. Wang and Y. Gui, *Coord. Chem. Rev.*, 2021, **438**, 213910.
7 R. Kumar, A. Pérez del Pino, S. Sahoo, R. K. Singh, W. K. Tan, K. K. Kar, A. Matsuda and E. Joanni, *Prog. Energy Combust. Sci.*, 2022, **91**, 100981.

8 L. Liu, P.-L. Taberna, B. Dunn and P. Simon, *ACS Energy Lett.*, 2021, **6**, 4311–4316.
9 M. Salanne, B. Rotenberg, K. Naoi, K. Kaneko, P.-L. Taberna, C. P. Grey, B. Dunn and P. Simon, *Nat. Energy*, 2016, **1**, 16070.
10 X. Zhang, X. Chen, T. Bai, J. Chai, X. Zhao, M. Ye, Z. Lin and X. Liu, *J. Mater. Chem. A*, 2020, **8**, 11589–11597.
11 F. Zhao, Y. Shi, L. Pan and G. Yu, *Acc. Chem. Res.*, 2017, **50**, 1734–1743.
12 S. Zhang, J. Zhu, Y. Qing, L. Wang, J. Zhao, J. Li, W. Tian, D. Jia and Z. Fan, *Adv. Funct. Mater.*, 2018, **28**, 1805898.
13 L. Yan, D. Li, T. Yan, G. Chen, L. Shi, Z. An and D. Zhang, *ACS Appl. Mater. Interfaces*, 2018, **10**, 42494–42502.
14 J. Mao, J. Iocozzia, J. Huang, K. Meng, Y. Lai and Z. Lin, *Energy Environ. Sci.*, 2018, **11**, 772–799.
15 Z. Qu, M. Shi, H. Wu, Y. Liu, J. Jiang and C. Yan, *J. Power Sources*, 2019, **410–411**, 179–187.
16 W. Fu, E. Zhao, X. Ren, A. Magasinski and G. Yushin, *Adv. Energy Mater.*, 2018, **8**, 1703454.
17 Y. Huang, H. Li, Z. Wang, M. Zhu, Z. Pei, Q. Xue, Y. Huang and C. Zhi, *Nano Energy*, 2016, **22**, 422–438.
18 Q. Meng, K. Cai, Y. Chen and L. Chen, *Nano Energy*, 2017, **36**, 268–285.
19 L. Li, K. Wang, Z. Huang, C. Zhang and T. Liu, *Nano Res.*, 2016, **9**, 2938–2949.
20 J. Gamby, P. Taberna, P. Simon, J. Fauvarque and M. Chesneau, *J. Power Sources*, 2001, **101**, 109–116.
21 H. Nishihara and T. Kyotani, *Adv. Mater.*, 2012, **24**, 4466.
22 J. Jiang, Y. Li, J. Liu, X. Huang, C. Yuan and X. W. D. Lou, *Adv. Mater.*, 2012, **24**, 5166–5180.
23 W. Wei, X. Cui, W. Chen and D. G. Ivey, *Chem. Soc. Rev.*, 2011, **40**, 1697–1721.
24 T. Lin, I. W. Chen, F. Liu, C. Yang, H. Bi, F. Xu and F. Huang, *Science*, 2015, **350**, 1508–1513.
25 Z. S. Wu, A. Winter, L. Chen, Y. Sun, A. Turchanin, X. Feng and K. Müllen, *Adv. Mater.*, 2012, **24**, 5130–5135.
26 M. Liu, B. Li, H. Zhou, C. Chen, Y. Liu and T. Liu, *Chem. Commun.*, 2017, **53**, 2810–2813.
27 M. Liu, Y. Song, S. He, W. W. Tjiu, J. Pan, Y. Y. Xia and T. Liu, *ACS Appl. Mater. Interfaces*, 2014, **6**, 4214–4222.
28 C. Cui, Y. Gao, J. Li, C. Yang, M. Liu, H. Jin, Z. Xia, L. Dai, Y. Lei, J. Wang and S. Wang, *Angew. Chem.*, 2020, **132**, 8002–8007.
29 Y. Li, Y. Shan and H. Pang, *Chin. Chem. Lett.*, 2020, **31**, 2280–2286.
30 S. Ghosh, S. Barg, S. M. Jeong and K. K. Ostrikov, *Adv. Energy Mater.*, 2020, **10**, 2001239.
31 H. Liu, F. Liu, Z. Qu, J. Chen, H. Liu, Y. Tan, J. Guo, Y. Yan, S. Zhao, X. Zhao, X. Nie, X. Ma, Z. Pei and M. Liu, *Nano Res. Energy*, 2023, **2**, e9120049.
32 V. Prabhakaran, B. L. Mehdi, J. J. Ditto, M. H. Engelhard, B. Wang, K. D. D. Gunaratne, D. C. Johnson, N. D. Browning, G. E. Johnson and J. Laskin, *Nat. Commun.*, 2016, **7**, 11399.
33 J. Lin, H. Liang, H. Jia, S. Chen, Y. Cai, J. Qi, J. Cao, W. Fei and J. Feng, *Inorg. Chem. Front.*, 2017, **4**, 1575–1581.
34 J. Yu, C. Yu, W. Guo, Z. Wang, S. Li, J. Chang, X. Tan, Y. Ding, M. Zhang, L. Yang, Y. Xie, R. Fu and J. Qiu, *Nano Energy*, 2019, **64**, 103921.
35 D. B. Amabilino, D. K. Smith and J. W. Steed, *Chem. Soc. Rev.*, 2017, **46**, 2404–2420.
36 E. A. Kovalenko, D. Y. Naumov and V. P. Fedin, *Polyhedron*, 2018, **144**, 158–165.
37 G. Cavallo, G. Terraneo, A. Monfredini, M. Saccone, A. Priimagi, T. Pilati, G. Resnati, P. Metrangolo and D. W. Bruce, *Angew. Chem., Int. Ed.*, 2016, **55**, 6300–6304.
38 T. Aida, E. W. Meijer and S. I. Stupp, *Science*, 2012, **335**, 813–817.
39 J. A. A. W. Elemans, A. E. Rowan and R. J. M. Nolte, *J. Mater. Chem.*, 2003, **13**, 2661–2670.
40 K. Liu, Y. Kang, Z. Wang and X. Zhang, *Adv. Mater.*, 2013, **25**, 5530–5548.
41 A. S. Weingarten, R. V. Kazantsev, L. C. Palmer, M. McClendon, A. R. Koltonow, A. P. S. Samuel, D. J. Kiebala, M. R. Wasielewski and S. I. Stupp, *Nat. Chem.*, 2014, **6**, 964–970.
42 Q. Wang, T. Xia, W. Wu, J. Zhao, X. Xue, C. Ao, J. Zhang, X. Deng, X. Zhang, W. Zhang and C. Lu, *Chem. Eng. J.*, 2022, **431**, 133228.
43 Z. Wang, Q. Zhang, S. Long, Y. Luo, P. Yu, Z. Tan, J. Bai, B. Qu, Y. Yang, J. Shi, H. Zhou, Z. Y. Xiao, W. Hong and H. Bai, *ACS Appl. Mater. Interfaces*, 2018, **10**, 10437–10444.
44 G. Vantomme and E. W. Meijer, *Science*, 2019, **363**, 1396–1397.
45 O. Dumele, J. Chen, J. V. Passarelli and S. I. Stupp, *Adv. Mater.*, 2020, **32**, 1907247.
46 T. Islam, M. M. Hasan, S. S. Akter, N. H. Alharthi, M. R. Karim, M. A. Aziz, M. D. Hossain and A. J. S. Ahammad, *ACS Appl. Polym. Mater.*, 2020, **2**, 273–284.
47 W. Fang, Y. Zhang, J. Wu, C. Liu, H. Zhu and T. Tu, *Chem. - Asian J.*, 2018, **13**, 712–729.
48 D. Zhao, Q. Zhang, W. Chen, X. Yi, S. Liu, Q. Wang, Y. Liu, J. Li, X. Li and H. Yu, *ACS Appl. Mater. Interfaces*, 2017, **9**, 13213–13222.
49 G. Li, H. Yang, D. Zuo, J. Xu and H. Zhang, *Int. J. Hydrogen Energy*, 2021, **46**, 13044–13049.
50 D. Das and S. Kurungot, *Energy Technol.*, 2020, **8**, 2000061.
51 G. Qin, M. Wang, L. Fan, X. Fang, D. Zhang, J. Liu, J. Qin, J. Shi, J. Yang and Q. Chen, *J. Power Sources*, 2020, **474**, 228602.
52 J. Yang, X. Yu, X. Sun, Q. Kang, L. Zhu, G. Qin, A. Zhou, G. Sun and Q. Chen, *ACS Appl. Mater. Interfaces*, 2020, **12**, 9736–9745.
53 J. N. Israelachvili, D. J. Mitchell and B. W. Ninham, *J. Chem. Soc., Faraday Trans. 2*, 1976, **72**, 1525.
54 S. I. Stupp, V. LeBonheur, K. Walker, L. S. Li, K. E. Huggins, M. Keser and A. Amstutz, *Science*, 1997, **276**, 384–389.
55 T. F. A. de Greef and E. W. Meijer, *Aust. J. Chem.*, 2010, **63**, 596.
56 I. D. Tevis, L. C. Palmer, D. J. Herman, I. P. Murray, D. A. Stone and S. I. Stupp, *J. Am. Chem. Soc.*, 2011, **133**, 16486–16494.

57 J. P. Hill, W. Jin, A. Kosaka, T. Fukushima, H. Ichihara, T. Shimomura, K. Ito, T. Hashizume, N. Ishii and T. Aida, *Science*, 2004, **304**, 1481–1483.
58 Y. Dong, Y. Wang, X. Zhang, Q. Lai and Y. Yang, *Chem. Eng. J.*, 2022, **449**, 137858.
59 W. Tian, H. Zhang, X. Duan, H. Sun, G. Shao and S. Wang, *Adv. Funct. Mater.*, 2020, **30**, 1909265.
60 B. Hu, X. Shang, P. Nie, B. Zhang, K. Xu, J. Yang, J. Qiu and J. Liu, *ACS Appl. Energy Mater.*, 2021, **4**, 6991–7001.
61 X. Zhang, X. Cui, C. H. Lu, H. Li, Q. Zhang, C. He and Y. Yang, *Chem. Eng. J.*, 2020, **401**, 126031.
62 X. Xie, X. He, H. Zhang, F. Wei, N. Xiao and J. Qiu, *Chem. Eng. J.*, 2018, **350**, 49–56.
63 R. Li, X. Li, J. Chen, J. Wang, H. He, B. Huang, Y. Liu, Y. Zhou and G. Yang, *Nanoscale*, 2018, **10**, 3981–3989.
64 R. Ma, X. Cui, X. Xu, Y. Wang, G. Xiang, L. Gao, Z. Lin and Y. Yang, *Nano Energy*, 2023, **108**, 108179.
65 Y. Huang, H. Cheng, D. Shu, J. Zhong, X. Song, Z. Guo, A. Gao, J. Hao, C. He and F. Yi, *Chem. Eng. J.*, 2017, **320**, 634–643.
66 H. Pan, Y. Zhang, Y. Pan, W. Lin, W. Tu and H. Zhang, *Chem. Eng. J.*, 2020, **401**, 126083.
67 L. Borchardt, D. Leistenschneider, J. Haase and M. Dvoyashkin, *Adv. Energy Mater.*, 2018, **8**, 1800892.
68 D. W. Wang, F. Li, M. Liu, G. Q. Lu and H. M. Cheng, *Angew. Chem., Int. Ed.*, 2009, **48**, 1525.
69 Q. Bai, Y. Shen, T. A. Asoh, C. Li, Y. Dan and H. Uyama, *Nanoscale*, 2020, **12**, 15261–15274.
70 O. A. Vasilyev, A. A. Kornyshev and S. Kondrat, *ACS Appl. Energy Mater.*, 2019, **2**, 5386–5390.
71 J. Min, X. Wen, T. Tang, X. Chen, K. Huo, J. Gong, J. Azadmanjiri, C. He and E. Mijowska, *Chem. Commun.*, 2020, **56**, 9142–9145.
72 Y. Li, Y. Du, G. Sun, J. Cheng, G. Song, M. Song, F. Su, F. Yang, L. Xie and C. Chen, *EcoMat*, 2021, **3**, e12091.
73 L. Yao, J. Lin, Y. Chen, X. Li, D. Wang, H. Yang, L. Deng and Z. Zheng, *InfoMat*, 2022, **4**, e12278.
74 J. Cui, J. Yin, J. Meng, Y. Liu, M. Liao, T. Wu, M. Dresselhaus, Y. Xie, J. Wu, C. Lu and X. Zhang, *Nano Lett.*, 2021, **21**, 2156–2164.
75 X. Cao, Z. Yin and H. Zhang, *Energy Environ. Sci.*, 2014, **7**, 1850–1865.
76 H. Cheng, L. Long, D. Shu, J. Wu, Y. Gong, C. He, Z. Kang and X. Zou, *Int. J. Hydrogen Energy*, 2014, **39**, 16151–16161.
77 H. Chen, X. Lu, H. Wang, D. Sui, F. Meng and W. Qi, *J. Energy Chem.*, 2020, **49**, 348–357.
78 X. Cui, L. Gao, S. Lei, S. Liang, J. Zhang, C. D. Sewell, W. Xue, Q. Liu, Z. Lin and Y. Yang, *Adv. Funct. Mater.*, 2021, **31**, 2009197.
79 X. Liu, X. Zhang, Y. Dou, P. Mei, X. Ma and Y. Yang, *Chem. Commun.*, 2021, **57**, 4966–4969.
80 L. Lai, Y. Zhao, S. Ying, L. Li, Z. Ma and L. Pan, *RSC Adv.*, 2018, **8**, 18714–18722.
81 Z. Li, Z. Xu, H. Wang, J. Ding, B. Zahiri, C. M. B. Holt, X. Tan and D. Mitlin, *Energy Environ. Sci.*, 2014, **7**, 1708–1718.
82 Y. Li, G. Wang, T. Wei, Z. Fan and P. Yan, *Nano Energy*, 2016, **19**, 165–175.
83 L. Yang, X. He, Y. Wei, H. Bi, F. Wei, H. Li, C. Yuan and J. Qiu, *Nano Res.*, 2022, **15**, 4068–4075.
84 L. N. Han, X. Wei, Q. C. Zhu, S. M. Xu, K. X. Wang and J. S. Chen, *J. Mater. Chem. A*, 2016, **4**, 16698–16705.
85 C. Liu, F. Yi, D. Shu, W. Chen, X. Zhou, Z. Zhu, R. Zeng, A. Gao, C. He and X. Li, *Electrochim. Acta*, 2019, **319**, 410–422.
86 W. Ai, J. Jiang, J. Zhu, Z. Fan, Y. Wang, H. Zhang, W. Huang and T. Yu, *Adv. Energy Mater.*, 2015, **5**, 1500559.
87 L. He, J. Liu, Y. Liu, B. Cui, B. Hu, M. Wang, K. Tian, Y. Song, S. Wu, Z. Zhang, Z. Peng and M. Du, *Appl. Catal., B*, 2019, **248**, 366–379.
88 H. Cheng, X. Zhou, A. Gao, F. Yi, D. Shu, X. Song, R. Zeng, C. He, S. Li and D. Zeng, *Electrochim. Acta*, 2018, **292**, 20–30.
89 H. Cheng, F. Yi, A. Gao, H. Liang, D. Shu, X. Zhou, C. He and Z. Zhu, *ACS Appl. Energy Mater.*, 2019, **2**, 4084–4091.
90 H. Cheng, B. Li, T. Meng, C. Liu and D. Shu, *Int. J. Energy Res.*, 2022, **46**, 18624–18633.
91 L. Zhang, H. Chen, X. Lu, Y. Wang, L. Tan, D. Sui and W. Qi, *Appl. Surf. Sci.*, 2020, **529**, 147022.
92 G. J. H. Lim, X. Liu, C. Guan and J. Wang, *Electrochim. Acta*, 2018, **291**, 177–187.
93 L. Tian, K. Xia, S. Wu, Y. Cai, H. Liu, X. Jing, T. Yang, D. Chen, X. Bai, M. Zhou and L. Li, *Electrochim. Acta*, 2019, **307**, 310–317.
94 J. Xu, Y. Sun, M. Lu, L. Wang, J. Zhang and X. Liu, *Sci. China Mater.*, 2019, **62**, 699–710.
95 F. Zhang, H. Yao, T. Chu, G. Zhang, Y. Wang and Y. Yang, *Chem. - Eur. J.*, 2017, **23**, 10293–10300.
96 G. Zhang, F. Zhang, H. Yao, Z. Liu and Y. Yang, *J. Mater. Chem. A*, 2017, **5**, 19036–19045.
97 K. Qi, R. Hou, S. Zaman, Y. Qiu, B. Y. Xia and H. Duan, *ACS Appl. Mater. Interfaces*, 2018, **10**, 18021–18028.
98 J. Xie, H. J. Peng, J. Q. Huang, W. T. Xu, X. Chen and Q. Zhang, *Angew. Chem., Int. Ed.*, 2017, **56**, 16223–16227.
99 F. Zhang, Y. Wang, T. Chu, Z. Wang, W. Li and Y. Yang, *Analyst*, 2016, **141**, 4502–4510.
100 Z. Wang, H. Yao, F. Zhang, W. Li, Y. Yang and X. Lu, *J. Mater. Chem. A*, 2016, **4**, 16476–16483.
101 Y. Liu, G. Li, Y. Guo, Y. Ying and X. Peng, *ACS Appl. Mater. Interfaces*, 2017, **9**, 14043–14050.
102 F. Zhang, G. Zhang, H. Yao, Z. Gao, X. Chen and Y. Yang, *Chem. Eng. J.*, 2018, **338**, 230–239.
103 F. Zhang, J. Ma, L. Bai, W. Xie, X. Wang and R. Zhang, *Appl. Surf. Sci.*, 2022, **601**, 154219.
104 Q. Li, H. Yao, F. Liu, Z. Gao and Y. Yang, *Electrochim. Acta*, 2019, **321**, 134682.
105 J. Ma, W. Li, X. Zhang, Y. Cheng and F. Zhang, *Appl. Surf. Sci.*, 2020, **507**, 145074.
106 H. Yao, G. Zhang, F. Zhang, W. Li, Y. Yang and L. Chen, *Mater. Today Energy*, 2017, **6**, 164–172.
107 J. Q. Shen, Y. Zhang, Z. M. Zhang, Y. G. Li, Y. Q. Gao and E. B. Wang, *Chem. Commun.*, 2014, **50**, 6017.
108 D. Wang, L. Liu, J. Jiang, L. Chen and J. Zhao, *Nanoscale*, 2020, **12**, 5705–5718.
109 K. Wang, K. Yu, J. Lv, M. Zhang, F. Meng and B. Zhou, *Inorg. Chem.*, 2019, **58**, 7947–7957.

110 W. J. Liu, G. Yu, M. Zhang, R. H. Li, L. Z. Dong, H. S. Zhao, Y. J. Chen, Z. F. Xin, S. L. Li and Y. Q. Lan, *Small Methods*, 2018, **2**, 1800154.
111 J. J. Zhu, R. Benages-Vilau and P. Gomez-Romero, *Electrochim. Acta*, 2020, **362**, 137007.
112 A. Guillén-López, N. D. Espinosa-Torres, A. K. Cuentas-Gallegos, M. Robles and J. Muñiz, *Carbon*, 2018, **130**, 623–635.
113 A. Anandan Vannathan, P. R. Chandewar, D. Shee and S. Sankar Mal, *J. Electroanal. Chem.*, 2022, **904**, 115856.
114 Z. Zheng, M. Li, Q. Zhou, L. Cai, J. F. Yin, Y. Cao and P. Yin, *ACS Appl. Nano Mater.*, 2021, **4**, 811–819.
115 F. M. Toma, A. Sartorel, M. Iurlo, M. Carraro, P. Parisse, C. Maccato, S. Rapino, B. R. Gonzalez, H. Amenitsch, T. Da Ros, L. Casalis, A. Goldoni, M. Marcaccio, G. Scorrano, G. Scoles, F. Paolucci, M. Prato and M. Bonchio, *Nat. Chem.*, 2010, **2**, 826–831.
116 S. Chen, Y. Xiang, M. K. Banks, C. Peng, W. Xu and R. Wu, *Nanoscale*, 2018, **10**, 20043–20052.
117 M. Wang, Y. Zhang, T. Zhang, Y. Li, M. Cui, X. Cao, Y. Lu, D. Peng, W. Liu, X. Liu, T. Wang and Y. Huang, *Nanoscale*, 2020, **12**, 11887–11898.
118 D. Kumar, A. Joshi, G. Singh and R. K. Sharma, *Chem. Eng. J.*, 2022, **431**, 134085.
119 G. Wang, T. Chen, C. J. Gómez-García, F. Zhang, M. Zhang, H. Ma, H. Pang, X. Wang and L. Tan, *Small*, 2020, **16**, 2001626.
120 L. Cui, K. Yu, J. Lv, C. Guo and B. Zhou, *J. Mater. Chem. A*, 2020, **8**, 22918–22928.
121 S. Hu, K. Li, X. Yu, Z. Jin, B. Xiao, R. Yang, H. Pang, H. Ma, X. Wang, L. Tan and G. Yang, *J. Mol. Struct.*, 2022, **1250**, 131753.
122 Z. Q. Shi, N. N. Ji, K. M. Guo and G. Li, *Appl. Surf. Sci.*, 2020, **504**, 144484.
123 X. Yu, S. U. Khan, Z. Jin, Q. Wu, H. Pang, H. Ma, X. Wang, L. Tan and G. Yang, *J. Energy Storage*, 2022, **53**, 105192.
124 K. Yang, A. Gao, H. Wu, F. Yi, D. Shu, X. Li and L. Xie, *Int. J. Energy Res.*, 2020, **44**, 7082–7092.
125 K. Yang, Z. Luo, D. Shu, F. Yi, Z. Zhu and A. Gao, *J. Electroanal. Chem.*, 2022, **908**, 116093.
126 J. Guo, H. Zhu, Y. Sun, L. Tang and X. Zhang, *J. Mater. Chem. A*, 2016, **4**, 4783–4789.
127 Y. Yang, Y. Wang, L. Zhao, Y. Liu and F. Ran, *Adv. Energy Mater.*, 2022, **12**, 2103158.
128 Y. Wang, X. Chu, Z. Zhu, D. Xiong, H. Zhang and W. Yang, *Chem. Eng. J.*, 2021, **423**, 130203.
129 F. Zhao, J. Bae, X. Zhou, Y. Guo and G. Yu, *Adv. Mater.*, 2018, **30**, 1801796.
130 Q. Zhang, Y. He, Y. Wang, J. Lu, N. Jiang and Y. Yang, *Adv. Funct. Mater.*, 2023, **33**, 2370027.
131 P. Kumari, K. Khawas, S. Nandy and B. K. Kuila, *Electrochim. Acta*, 2016, **190**, 596–604.
132 S. Li, A. Gao, F. Yi, D. Shu, H. Cheng, X. Zhou, C. He, D. Zeng and F. Zhang, *Electrochim. Acta*, 2019, **297**, 1094–1103.
133 Y. Zhao, B. Liu, L. Pan and G. Yu, *Energy Environ. Sci.*, 2013, **6**, 2856.
134 Y. Guo, J. Bae, Z. Fang, P. Li, F. Zhao and G. Yu, *Chem. Rev.*, 2020, **120**, 7642–7707.
135 S. Naficy, J. M. Razal, G. M. Spinks, G. G. Wallace and P. G. Whitten, *Chem. Mater.*, 2012, **24**, 3425–3433.
136 M. Ma, L. Guo, D. G. Anderson and R. Langer, *Science*, 2013, **339**, 186–189.
137 W. Li, F. Gao, X. Wang, N. Zhang and M. Ma, *Angew. Chem., Int. Ed.*, 2016, **55**, 9196–9201.
138 F. Gao, J. Song, H. Teng, X. Luo and M. Ma, *Chem. Eng. J.*, 2021, **405**, 126915.
139 J. J. Alcaraz-Espinoza, G. Ramos-Sánchez, J. H. Sierra-Uribe and I. González, *ACS Appl. Energy Mater.*, 2021, **4**, 9099–9110.
140 X. Zhou, T. Meng, F. Yi, D. Shu, D. Han, Z. Zhu, A. Gao, C. Liu, X. Li, K. Yang and H. Yi, *J. Power Sources*, 2020, **475**, 228554.
141 Q. Liu, A. Gao, Y. Huang, F. Yi, H. Cheng, S. Zhao, H. Chen, R. Zeng, Z. Sun, D. Shu and X. Song, *J. Alloys Compd.*, 2019, **777**, 1176–1183.
142 R. Zhao, K. Li, R. Liu, M. Sarfraz, I. Shakir and Y. Xu, *J. Mater. Chem. A*, 2017, **5**, 19098–19106.
143 M. C. G. Saborío, S. Lanzalaco, G. Fabregat, J. Puiggalí, F. Estrany and C. Alemán, *J. Phys. Chem. C*, 2018, **122**, 1078–1090.
144 G. Li, X. Zhang, M. Sang, X. Wang, D. Zuo, J. Xu and H. Zhang, *J. Energy Storage*, 2021, **33**, 101931.
145 S. Xu, X. Liang, K. Ge, H. Yuan and G. Liu, *ACS Appl. Energy Mater.*, 2022, **5**, 2929–2936.
146 Z. Wang, X. Han, Y. Wang, K. Men, L. Cui, J. Wu, G. Meng, Z. Liu and X. Guo, *Front. Mater. Sci.*, 2019, **13**, 54–63.
147 J. Gačanin, J. Hedrich, S. Sieste, G. Glaßer, I. Lieberwirth, C. Schilling, S. Fischer, H. Barth, B. Knöll, C. V. Synatschke and T. Weil, *Adv. Mater.*, 2019, **31**, 1805044.
148 F. Mo, Q. Li, G. Liang, Y. Zhao, D. Wang, Y. Huang, J. Wei and C. Zhi, *Adv. Sci.*, 2021, **8**, 2100072.
149 E. Feng, W. Gao, J. Li, J. Wei, Q. Yang, Z. Li, X. Ma, T. Zhang and Z. Yang, *ACS Sustainable Chem. Eng.*, 2020, **8**, 3311–3320.
150 B. Pal, S. Yang, S. Ramesh, V. Thangadurai and R. Jose, *Nanoscale Adv.*, 2019, **1**, 3807–3835.
151 V. Jose, J. M. V. Nsanzimana, H. Hu, J. Choi, X. Wang and J. Lee, *Adv. Energy Mater.*, 2021, **11**, 2100157.
152 O. Borodin, J. Self, K. A. Persson, C. Wang and K. Xu, *Joule*, 2020, **4**, 69–100.
153 H. Zhang, X. Liu, H. Li, I. Hasa and S. Passerini, *Angew. Chem., Int. Ed.*, 2021, **60**, 598–616.
154 C. Tang, M. Li, J. Du, Y. Wang, Y. Zhang, G. Wang, X. Shi, Y. Li, J. Liu, C. Lian and L. Li, *J. Colloid Interface Sci.*, 2022, **608**, 1162–1172.
155 H. Li, L. Ma, C. Han, Z. Wang, Z. Liu, Z. Tang and C. Zhi, *Nano Energy*, 2019, **62**, 550–587.
156 L. Dong, X. Ma, Y. Li, L. Zhao, W. Liu, J. Cheng, C. Xu, B. Li, Q. H. Yang and F. Kang, *Energy Storage Mater.*, 2018, **13**, 96–102.
157 X. Gong, J. Chen and P. S. Lee, *Batteries Supercaps*, 2021, **4**, 1527–1528.
158 Z. Wang, M. Zhang, W. Ma, J. Zhu and W. Song, *Small*, 2021, **17**, 2100219.
159 H. Yang, J. Zhang, J. Yao, D. Zuo, J. Xu and H. Zhang, *J. Energy Storage*, 2022, **53**, 105089.